NTNU
Norwegian University of
Science and Technology

Study end surfaces of GaAsSb NW grown on graphene by electron microscopy

Johanna Neumann

Norwegian University of Science and Technology
Department of Physics

Abstract

III-V nanowires (NWs) are attractive for solar cells. Through the composition of the NWs, their bandgap and hence their electronic properties can be tuned, for example, to optimise absorption so that most of the Sun's radiation is used.

In this study, compositional analysis of Ga-As-Sb, Al-Ga-N, In-Ga-N systems has been done using Scanning transmission electron microscopy (STEM) and Energy Dispersive X-ray Spectroscopy (EDS) with the aid of the Python-based Hyperspy library for a more transparent and possibly better compositional analysis. This includes setting up an analysis routine based on the quantification method called zeta method intruduced by Watanabe & Williams, but not available yet in commercial software packages.

The required ζ-factor has been estimated experimentally for the elements Ga, As, Sb, Al, N, In, C, O, Si on the used JEOL JEM2100F with an 80 mm^2 silicon drift detector and the ζ-method compared to the classical Cliff-Lorimer method. Different reference samples with known thickness and composition were used for this step.

Tilt effects on the zeta-factor quantification were studied with GaAs NWs and the Ga catalyst droplet of GaAsSb NWs. When the holder was tilted to negative X-tilts, the ζ-factor increased. In the range between 0° and 35° tilt, the ζ-factors were constant indicating no detector shadowing.

For ζ calibration and mapping, a positive tilt was used to avoid shadowing effects. Quantitative compositional maps have been calculated of areas within GaAsSb, AlGaN and InGaN NWs that contain a heterostructure. These heterostructures could have a varying thickness or composition in the direction of the electron beam Using the EDS spectra images, thickness maps could be constructed for areas where the composition was known.

Further refinements to the zeta method have to be made, especially finding good calibration specimens with exactly known thicknesses.

Preface

Work for this thesis was performed at the TEM Gemini Centre. It is a master thesis following up a specialisation project within the Master 'Sustainable Energy Engineering, Solar Cell Systems and Materials' within the Department of Physics (IFY) at the Norwegian University of Science and Technology (NTNU) carried out from January to June 2018.

The NWs analysed here, were grown in the MBE lab at the Department of Electronics and Telecommunication (IET) by Dr Dingding Ren. Reference samples were grown by Mazid Munshi and Andreas Liudi Mulyo, a FIB sample was prepared by Per Erik Vullum. Supervision of the project was done by Professor Antonius T. J. Van Helvoort at NTNU, Trondheim, and co-supervisors Christian Danvad Damsgaard and Jakob Birkedal Wagner at DTU, Kopenhagen.

Thanks to my extraordinary supervisor Antonius T. J. Van Helvoort for guidance, help and constructive feedback, thanks to Postdoc Dingding Ren for sample preparation, Ragnhild Sæterli and Bjørn Gunnar Soleim for teaching me how to operate the TEM, and the TEM group with their weekly Friday lunch seminar. Thanks to NTNU Nanolab who granted me access to use the SEM APREO.

Also thanks to my fellow students Annika, Carolyn, Kevin and Ruby, and my family for all their support.

Trondheim, 25th June 2018

Johanna Neumann

Nomenclature

BF	Bright-Field imaging in TEM
CCD	Charge-Coupled Device
DP	Diffraction Pattern in TEM
EDS	Energy Dispersive X-ray Spectroscopy
ETD	Everhart-Thornley detector
FFT	Fast Fourier Transformation
GaAsSb	Gallium Arsenide Antimonide
HAADF	High-Angle-Annular-Dark-Field imaging in TEM
HRTEM	High resolution TEM
MBE	Molecular Beam Epitaxy
NMF	Non-negative matrix factorisation
NW	Nanowire
PCA	Principle component analysis
SAED	Selected area energy diffraction
SEM	Scanning electron microscopy
SQ	Shockley-Queisser
STEM	Scanning transmission electron microscopy

TEM	Transmission electron microscopy
VLS	Vapour-Liquid-Solid
ZB	Zinc-Blende

Contents

Chapter 1

Introduction

With an increasing number of people and energy need, renewable energy resources are necessary in addition to fossil fuels. The sun is the most abundant of the renewable energies. Therefore, solar cells, which produce electricity by converting the sun's radiation, can be promising as future sustainable energy source. There are different generations and types of solar cells on the market. The first generation includes silicon solar cells, which are dominating the market and are most often used on house roofs. The second generation are thin film solar cells and the third are newer solar cells based on other systems such as organic solar cells, quantum dot solar cells or nanowire solar cells. The latter is a novel and promising solar cell consisting of NWs as the active material with the pn-junction. While efficiencies for NW solar cells are reaching half the Shockley-Queisser limit (SQ-limit) [Otnes and Borgström (2017)], there are theoretical studies that predict that for NWs the Shockley-Queisser limit (SQ-limit) can be surpassed [Krogstrup et al. (2013)]. This limit is the maximum efficiency of a single pn-junction and depends on the bandgap of the pn-junction. Further optimisation of NW material and device structure are required to reach towards the maximum possible.

There are several advantages using NWs as active component in a solar cell. With NWs, the distance between them can be adjusted to the order of the wavelength of light to optimise absorption. This light trapping increases the efficiency [Otnes and Borgström (2017)]. Due to the space between small diameter NWs, the matching criteria of the lattice spacing of the NWs and of the substrate is relaxed. The diameter of the NW is very small, the free surface area can reduce the stress due to lattice mismatching. This allows

alternative (i.e. cheaper) substrates to be used and limits the formation of misfit dislocations that limit the efficiency of thin film based solar cells. Another advantage of NW solar cells is a short distance between the pn-junction and the outer contact. This reduces unwanted e^-h^+ recombinations, and increases thereby the efficiency.

In order to use most of the solar radiation from the solar spectrum, the bandgap of the NWs can be tuned. Tuning the bandgap of a material is possible by tailoring its composition [Papadopoulos (2014)]. To be able to grow NWs with a particular composition, it is necessary to measure the composition. One option of analysing composition in thin material ($<$10-200 nm) is by energy dispersive x-ray spectroscopy (EDS) in a transmission electron microscope (TEM). There are two main methods in calculating the composition from measured x-ray intensities. One is the Cliff-Lorimer method, (CL method), [Cliff and Lorimer (1975)]. This is a long-used method for thin films, which relates the intensity to the composition by a ratio of two elements. The newer one is the ζ method [Watanabe and Williams (2006)]. This method takes additionally the specimen mass-thickness and the electron dose into account. Although the zeta method is generally seen as potentially the more accurate method, it is seldom used as it requires probe measurements in addition to EDS, the constants have to be calibrated for each system by the user and the method is not yet available in commercial and easy to use packages.

In this thesis, quantitative EDS is used to analyse the composition at the top and bottom parts of several NWs with different compositions. These ends will be a crucial part of the final devices and their electronic characteristics, partly dependent on their composition, which might dominate the device performance. The aim is to find the composition of parts of the NW with a high accuracy using both the CL method and the ζ method. As the latter is not yet implemented in most commercial EDS software packages, the method had to be implemented and calibrations taken for the used TEM-EDS system. In this project, first the theory necessary to understand imaging using SEM and TEM is introduced, followed by an elementary introduction to NWs, the CL method and the ζ method, Chapter 2. In Chapter 3, there is an experimental overview of how the samples were prepared and what hardware and software were used. After that, results are presented and discussed. A conclusion summarises the findings and further work is suggested.

Chapter 2

Theory

The theory chapter is devided into four parts, first it describes how electrons are diffracted in crystals, then an introduction in electron microscopy, followed by EDS in TEM describing the principal component analyser as data treatment and the two methods: CL and ζ, and lastly about III-V NW.

2.1 Crystallographic diffraction

The interplanar distance for a cubic system for a crystal plane (hkl) can be calculated, [Williams and Carter (2009)]:

$$d_{hkl} = \frac{1}{\sqrt{\frac{h^2}{a_1^2} + \frac{k^2}{a_2^2} + \frac{l^2}{a_3^2}}} \tag{2.1}$$

with the primitive lattice vectors a_1, a_2 and a_3.

When an incident plane wave is in phase with the scattered plane wave, the Bragg condition is fulfilled:

$$2dsin(\theta) = n\lambda \tag{2.2}$$

with the distance between two crystal planes d, and the scattering angle θ. The crystal plane distance d and the scattering angle θ have a reciprocal relationship. In a more general visual description, with the incoming electron vector $\boldsymbol{k}$ and diffracted $\boldsymbol{k'}$, the Ewald sphere, Fig. 2.1, shows the difference in phase with the scattering vector $\Delta\boldsymbol{k}=\boldsymbol{k'}-\boldsymbol{k}$.
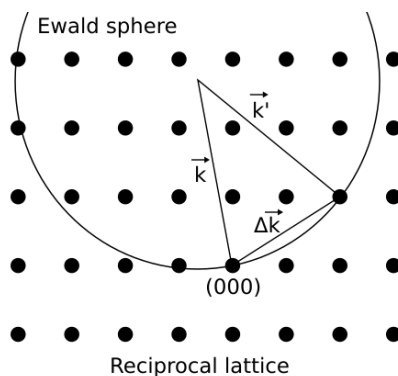
Figure 2.1: Schematics of the Ewald sphere in the reciprocal lattice.

The structure factor (for a perfect crystal) measures the amplitude scattered by a unit cell:

$$F = \sum_j f_j exp(-i\mathbf{G}\mathbf{r}_j) = \sum_j f_j exp(-2\pi i(hx_j + ky_j + lz_j)) \qquad (2.3)$$

with atomic form factors f_j and reciprocal lattice vector $\mathbf{G}$. The intensity I and scattering amplitude A have the following relationship for kinematic diffraction with the structure factor with N unit cells in the crystal:

$$I \propto A^2 = N^2 F^2 \qquad (2.4)$$

$|F^2(\theta)|$ is proportional to the scattered intensity I. σ describes the scattering cross section, $f(\theta)$ is the atomic scattering cross section. It is the strength of the scattering and depends inversely on the scattering angle θ (where an atom is the scattering center).

2.2 Electron Microscopy

Basics for electron microscopy, interaction volume, contrast and diffraction are described in this section. There are different types of electron microscopy and electron beam techniques. SEM and TEM are the ones used here.

2.2.1 Electron-Matter Interaction

When electrons hit a sample with an energy E, they interact with the sample in different ways. Fig. 2.2 shows electrons and photons that can be measured

after a high kV-beam is directed onto a material. In the SEM, the sample has a thickness in the μm range. Electrons do not have enough energy to pass through it, therefore, electrons can only escape the sample through the surface where the beam penetrates. In the TEM, on the other hand, the sample is around 100 nm thin, so the electrons penetrate the sample and scatter once or not at all. Dynamic scattering, more than one scattering event, is likely as the electron-matter interaction is strong. It becomes more important when the sample is thicker.
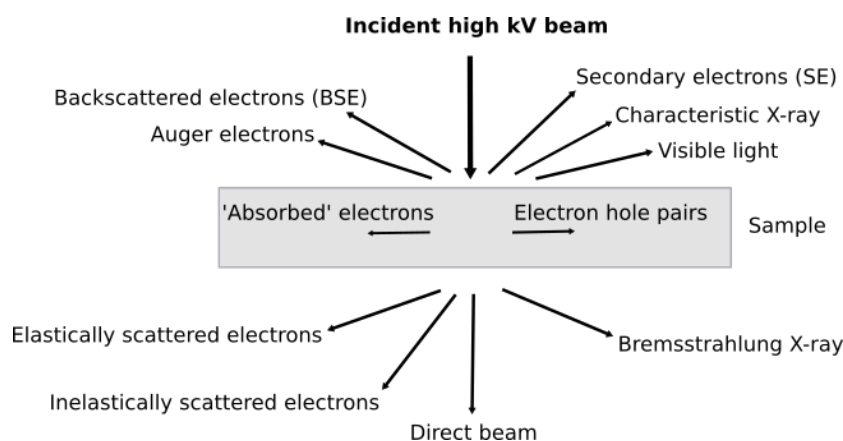
Figure 2.2: Interaction between beam electrons and matter.

When detecting electrons and X-rays, it is important to know that electrons are charged and, therefore, scatter much more strongly than X-rays.

2.2.2   Contrast in SEM

For surface topography analysis, a scanning electron microscope (SEM) can be used. It is a point scanning technique which means that every point of a sample area has to be scanned to create an image of this area. The typical magnification ranges from 10 to 10,000 x, the electron energy ranges between 1 and 30 keV. The SEM consists of an electron source, a long beam column with apertures and lenses, the sample and detectors. Since electrons travelling through the column will interact with atoms, the whole apparatus needs to be in vacuum, thus a vacuum pump is necessary.

As an electron source a field emission gun (FEG) is used. After leaving the source, electrons travel through a condensor aperture followed by a condensor lens, which focuses the beam (reduces beam diameter). Further down there is an objective aperture and an objective lens to focus the beam onto a specific spot on the sample.

When the beam hits the specimen, the primary electrons (beam electrons) interact with the specimen. The beam electrons can hit electrons out of the specimen while entering the sample. These are secondary electrons of type one (SE1). When the primary backscattered electrons hit electrons out of the sample while exiting the sample, these secondary electrons are of type two (SE2). The electrons from the beam that have enough energy left to exit the sample are called backscattered electrons (BSE), see Fig. 2.3a.
In addition to electrons, electromagnetic waves can escape the sample. When an electron gets hit out of an atom it leaves a hole behind. The atom is excited and emits either characteristic X-rays when an electron from an outer shell falls into the hole. Instead of X-ray radiation, the atom can also emit an Auger electron from a third shell.
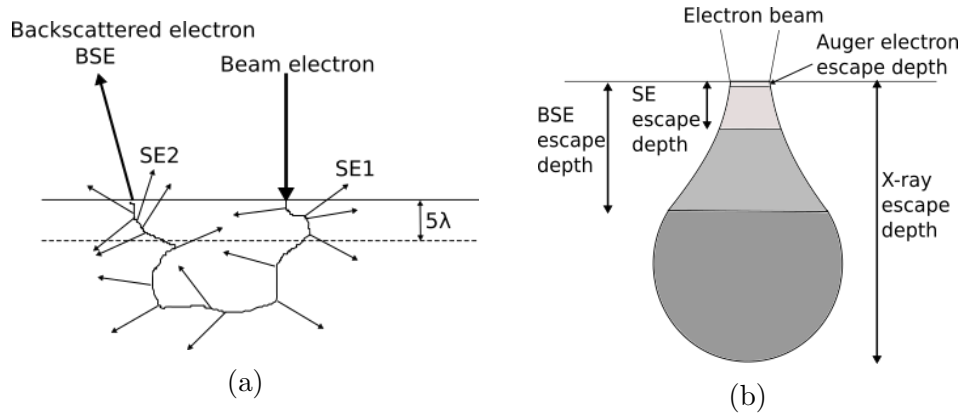
Figure 2.3: (a) Path of an electron through thick material. λ is the free mean path of secondary electrons. After [Goldstein et al. (2003)] (b) Interaction volume when an electron beam hits a material surface.

All secondary and backscattered electrons with enough energy to leave the sample can be detected, for example, with an Everhart-Thornley detector (ET-detector). It has a grid in front of it that can be biased positive or

negative. If it is biased negative, it prevents SE from entering the detector, and only BSE can enter since they have a much higher energy. If the grid is biased positively, it attracts SE, who have energies below 50 eV. In this project, the ET detector was used with positive bias.

There are also scattered electrons of type 3 (SE3) that can be detected by the ET-detector. Those electrons originate from the polepiece or the chamber walls of the microscope when they get hit by BSE.

Looking at the interaction volume, see Fig. 2.3b, it can be seen that scattered electrons of different types originate from different depth due to their varying energies. Auger electrons only come from close to the surface, SEs come from a bit deeper regions than Auger electrons, and BSEs come from even deeper regions in the sample. Only X-rays originate from the entire interaction volume.

When interpreting SEM images, two effects need to be considered; If the primary electron beam hits a flat surface, a smaller part of the interaction volume is close to the surface than when the beam hits an uneven surface. In case of the uneven surface, more SE can escape the sample and this part of the surface is seen as a brighter area. This is called the edge-effect. Another effect is the shadow-effect. This happens because the ET-detector is situated not directly above the sample but further to one side of the sample. The electrons that escape from the uneven surface facing the detector are more likely to reach the detector than those escaping an uneven surface facing away from the detector. This is in analogy with the sun shining onto an uneven surface creating shadows. Having these two effects in mind, images can be analysed.

The signal per probe position is displayed, forming the image.

2.2.3   TEM hardware

In the TEM, the electron energy ranges between 100-300 keV. The TEM has an electron gun, in this study a warm field-emission (Schottkey) gun crystal, several lenses, deflectors and apertures to guide the electron beam to the sample and detectors. The lenses are electromagnetic. Because the beam are moving electrons in a magnetic field and therefore experience a Lorentz force,

Filament

Electron gun 1st beam deflector: Gun shift

Electron gun 2nd beam deflector: Gun tilt

C1   1st condensor lens: Spot size

C2   2nd condensor lens: C-O lens (not user controlled)

C3   3rd condensor lens: Brightness

Condensor lens stigmator: CL stig

Spot alignment (not user controlled)

Condensor lens 1st deflector: Beam shift

Condensor lens 2nd deflector: Beam tilt

Condensor mini lens: alpha selector

Specimen ----------------------------------

Objective lens stigmator: Obj stig

OL   Objective lens: focus
Objective mini lens (at low magnification, not user controlled)

Image shift 1st deflector: Image shift

Image shift 2nd deflector: Image tilt

Intermediate lens stigmator: IL stig

IL1   1st intermediate lens: Mag/SaDiff

IL2   2nd intermediate lens: Magnification/ Camera length

IL3   3rd intermediate lens: Rotation (not user controlled)

Projector lens deflector: PLA

Projector lens (not user controlled)

Figure 2.4: Schematic layout of the TEM column, apertures are not included.

they spiral through the TEM column. The sample is very thin (typically $<$ 100 nm), so most electrons are transmitted through the sample. Fig. 2.4 shows the schematic of the TEM without apertures.

2.2.4 Contrast in TEM

When the electron beam hits the specimen, electron waves are scattered by the specimen, which leads to TEM image contrast. Both the amplitude and the phase of the electron wave can be altered when it traverses the specimen. This change in wave amplitude and phase can result in image contrast.

Amplitude contrast is devided in mass-thickness contrast, which originates from incoherent elastic (Rutherford) scattering of the electrons, and in diffraction contrast, which is Bragg diffraction, which is elastic scattering of coherent beams at small angles. Both contrasts lead to thickness fringes and bending contours.
Bright field (BF) and Dark field (DF) imaging are the two most basic modes in the TEM. In BF imaging the objective lens aperture is centered around the central beam. This way only electrons from the direct beam contribute to the image formation. The image on the screen appears as dark and the background as bright. At the objective lens, all scattered electrons from one point in the sample are focused to one point on the screen, see solid lines in Fig. 2.5. The objective aperture is inserted, the SAD aperture is removed. In DF imaging the objective lens aperture selects part of the scattered electrons and excludes the direct beam. The sample appears bright, the background dark.

Phase contrast is due to interference of beams after the sample and can be seen when more than one beam contributes to the image. This contrast leads to lattice fringes. One specific case of phase contrast are Moiré patterns. They are formed by interference by two lattice planes with similar periodicities or planes that are slightly rotated against each other.
High resolution images are formed without the objective lens and thus includes the direct and diffracted beams. Therefore phase contrast can be seen in HRTEM images. HRTEM images are used to image lattice spacing and symmetry to identify the crystal phase, growth and facet directions and possible lattice defects.
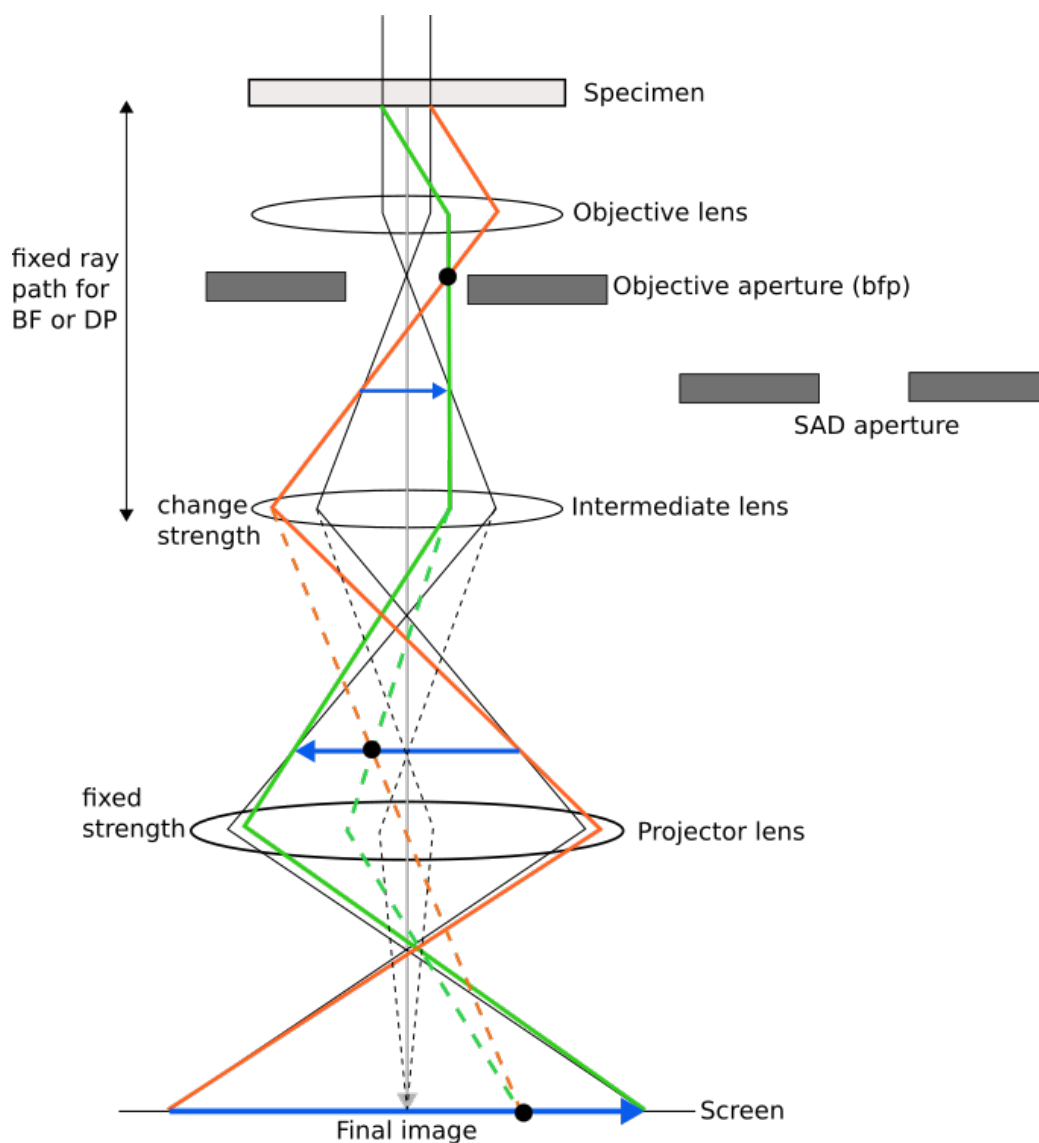
Figure 2.5: Electron paths for BFTEM and SAED. The solid lines represent the BF TEM. The dashed lines show the SAED, if the objective aperture is removed and the SAD aperture inserted. The blue arrows show the images at different positions in the TEM in BF mode, and the black spots the DP in SAED mode, adapted from (Williams and Carter, 2009).

One other aspect that can influence the resolution in TEM images are imperfections in the electromagnetic lenses. That can be astigmatism, spherical aberration and chromatic aberration. The astigmatism can easily be corrected by an octapole. Spherical aberration limits the performance and can be partly counterbalanced by defocus or the use of correctors. Chromatic aberration has an effect due to the energy spread in the beam or after interaction with the specimen, and are for conventional TEM not the limiting factor for ultimate resolution.

2.2.5   Diffraction in TEM

In diffraction mode, the objective aperture is removed and the SAD aperture is inserted making diffraction spots visible on the screen. In the backfocal plane of the objective lens, all electrons scattered through the sample with the same angle are focused in one point, see Fig. 2.5.
The diffraction spots can be linked to lattice planes in the crystal, because the real space and reciprocal space are related. The following equation is valid [Williams and Carter (2009)]:

$$Rd_{hkl} = \lambda L \tag{2.5}$$

with the camera length L (microscope parameter), the interplanar distance d_{hkl}, the wavelength of the beam electrons λ, and the distance between a diffraction spot and the central spot (000) R. The product λL is constant in a diffraction image. From this and Equation 2.1, the relation between two distances R_i and the angle between two diffraction spots and the (000) spot can be calculated and the respective crystal structure be found. Apart from crystal structure, a diffraction pattern can also give information about possible crystal defects such as twinning, see Section 2.4.3.

2.2.6   STEM

The conventional TEM uses a parallel beam onto the sample. In scanning transmission electron microscopy (STEM), the beam is converged to a spot onto the specimen. This spot is then scanned across the surface of the specimen. The scattered signal can be collected at different angles, for example, high angle annular dark field (HAADF) STEM. It is advantageous to record EDS spectroscopy per point using STEM mode to construct spectral images

or line scans.

HAADF STEM images have a strong Z-contrast and coherent diffraction effects are excluded if the starting angle is large enough (for 200 kV medium Z element > 50 mrad). If the annular HAADF detector is large enough, an incoherent image is formed. The scatter angle is selected by controlling the camera length using the intermediate lenses. BF STEM is also possible and has a contrast similar to BF TEM. As with SEM (Section 2.2.2), the collected signal is recorded per beam position.

2.3 Methods for quantitative EDS analysis

For thin and light samples, the counts in the EDS detector can be small and the S/N ratio needs to be improved. For this, the principle component analyser is briefly described. As a following step, for quantitative EDS mapping, two methods for thin film specimen can be used and are presented thereafter. These are the CL- and ζ-methods.

2.3.1 Principal component analysis (PCA)

One way of improving the signal to noise (S/N) ratio is by in increasing the signal. This is possible with a bigger probe size in the TEM, because increasing the electrons that hit the sample also increases the number of interaction with the sample and the number of x-rays detected. There is a maximum amount of electrons that a sample can tolerate without getting damaged (i.e. critical dose). This limit is low for small particles such as small NWs or NWs with light elements such as nitrogen. If the signal cannot be increased further and the data is still poorly, the noise can be reduced. One option to reduce the noise is to bin the data. This leads to high loss in spatial resolution. For an evenly thick sample with homogeneous composition, this can be a good solution. For a sample with changing thickness and composition, a high resolution is desired. This leaves another option of noise reduction by using the principal component analysis, PCA. This is machine learning, where the algorithm finds a number of the most frequent spectra (called scree plot) and throws away the rest assuming that these spectra contain noise only. PCA was successfully used to denoise EDS spectra images amongst others in [Jany et al. (2017)].
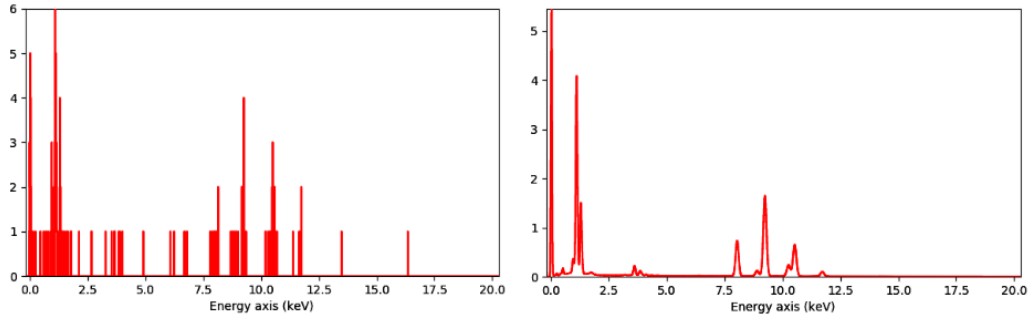
Figure 2.6: One raw spectrum of GaAsSb top crystal (left) and using PCA (right). The zero peak gets cut out for further data processing.

2.3.2 Cliff-Lorimer-Method

First introduced by [Cliff and Lorimer (1975)], the Cliff-Lorimer method (CL-method) is a simple method but it does not assume any absorption. For light elements this can be problematic. For evenly thick samples with homogeneous composition, this classical method works very well. It relates the intensities and compositions of two elements with a proportionality factor k:

$$\frac{C_A}{C_B} = k_{AB} \frac{I_A}{I_B} \tag{2.6}$$

with C_i the composition of element i in weight percent, I_i the x-ray intensity of element i above background and k_{ij} the Cliff-Lorimer factor, which can be determined experimentally (difficult as good standards are needed and exactly the same illumination conditions) or theoretically (most used to date) [Goldstein et al. (2003), Williams and Carter (2009)].

2.3.3 ζ-Method

A newer and more precise method for EDS quantification was introduced by [Watanabe and Williams (2006)] as the ζ-method. This method takes the mass-thickness and electron dose into account, and has the possibility of including absorption correction.
The X-ray intensity I_A of element A in an analysed volume is proportional

to the mass-thickness (ρt), composition C_A and electron dose D_e:

$$\rho t = \xi_A I_A / (C_A D_e) \tag{2.7}$$

where the electron dose D_e is:

$$D_e = I_p \tau N_e \tag{2.8}$$

with the probe current I_p, the acquisition time τ and the number of electrons $N_e[\#/e]$. For a relative composition of two elements (C_A/C_B), the mass-thickness ρt eliminates and makes absorption correction easier.

With two elements, A and B, $C_A + C_B = 1$ and Eq. 2.7, three equations can be formed for calculating the mass-thickness or the composition:

$$\rho t = \frac{\zeta_A I_A + \zeta_B I_B}{D_e}, \ C_A = \frac{\zeta_A I_A}{\zeta_A I_A + \zeta_B I_B}, \ C_B = \frac{\zeta_B I_B}{\zeta_A I_A + \zeta_B I_B} \tag{2.9}$$

These can be expanded to more than two elements. The zeta constant needs to be calibrated for each TEM-EDS system, however, pure samples with known composition and thickness are necessary. For the zeta method, the probe current has to be measured during the experiment. The two big advantages are that 1) the effect of thickness or density variation is corrected in the composition analysis and 2) an absorption correction A, based on tabulated absorption coefficients and less complicated than for the CL-method, can be applied.
If also absorption correction A is taken into account, Eqs. 2.9 result in

$$\rho t = \sum_j^N \frac{\zeta_j I_j A_j}{D_e}, \ C_A = \frac{\zeta_A I_A A_A}{\sum_j^N \zeta_j I_j A_j}, \ C_N = \frac{\zeta_N I_N A_N}{\sum_j^N \zeta_j I_j A_j} \tag{2.10}$$

2.4 III-V NWs

III-V NWs consist of elements from the third to the fifth group of the periodic table. The following sections introduce them.

2.4.1 NW Synthesis

NW growth with the Molecular-Beam-Epitaxy (MBE) machine uses UHV to achieve ultra high purity. Shutters can be opened to let specific elements flow towards a sample, which can be heated and rotated. Growth rates can be accurately controlled and in-situ characterisation can be done using reflection high-energy electron diffraction (RHEED). Fig. 2.7 shows the MBE growth as a schematic.
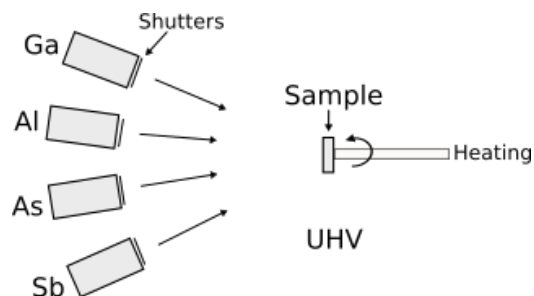
Figure 2.7: Schematic of MBE growth set-up.

In the vapour-liquid-solid (VLS) method there is a vapour phase, a liquid phase and a solid phase. Where these three phases meet, the growth happens. [Wagner and Ellis (1964)] explains the process using Au as catalyst. Here the growths are self-catalyzed.

In the MBE machine, the vapour phase is supplied by the machine. The liquid phase is in the beginning a droplet on the sample. Then the droplet moves up while the NW is growing underneath it. The solid phase is first the seed particle and then the NW. Fig. 2.8 is a schematic of the VLS growth method.
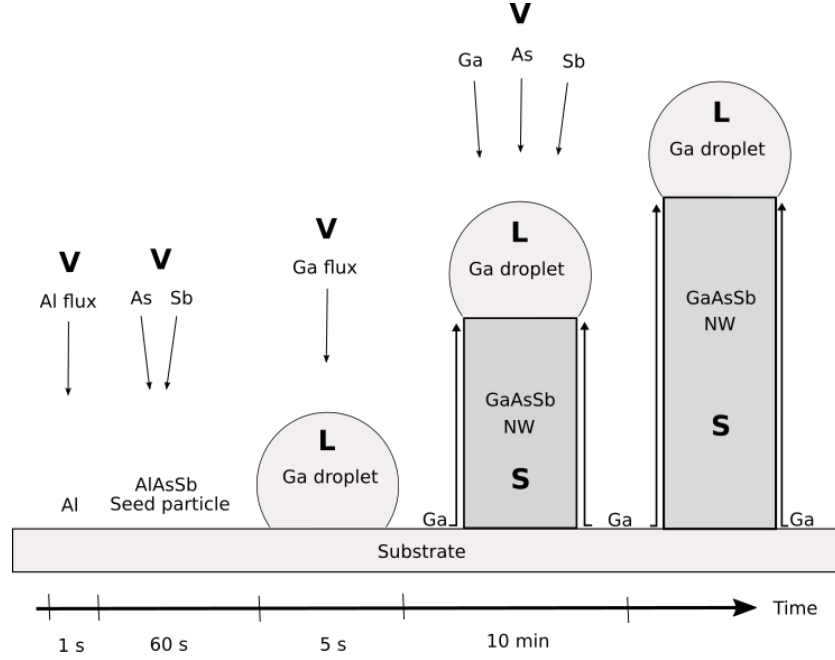
Figure 2.8: VLS growth of a NW. The time of the VLS growth steps is not specific, the time slots in this image are the ones used in growing the GaAsSb sample B analysed in this thesis. V stands for vapour, L for liquid and S for solid.

2.4.2 NW Geometry and Morphology

Ga-As-Sb. Both GaAs and GaSb have fcc crystal structure. For GaAs$_{1-y}$Sb$_y$, there are two fcc crystals together, an fcc crystal with two different base atoms. This is called the zinc-blende (ZB) structure. If the Ga atom sits in the (0,0,0) position, the As or the Sb is in the $[\frac{1}{4}, \frac{1}{4}, \frac{1}{4}]$ position.
The structure factor, which is used in the indexing of diffraction patterns, is:

$$F_{hkl} = f_{Ga}\left[1 + e^{-2\pi i(\frac{1}{2}h + \frac{1}{2}k)} + e^{-2\pi i(\frac{1}{2}k + \frac{1}{2}l)} + e^{-2\pi i(\frac{1}{2}h + \frac{1}{2}l)}\right] + \tag{2.11}$$
$$f_{As}\left[e^{-2\pi i(\frac{1}{4}h + \frac{1}{4}k + \frac{1}{4}l)} + e^{-2\pi i(\frac{3}{4}h + \frac{3}{4}k + \frac{3}{4}l)} + e^{-2\pi i(\frac{1}{4}h + \frac{3}{4}k + \frac{3}{4}l)} + e^{-2\pi i(\frac{3}{4}h + \frac{1}{4}k + \frac{3}{4}l)}\right]$$

As a consequence, there are strong reflections, f.ex., for (400): I=F^2= 4(f$_{Ga}$+f$_{As}$) and weaker ones, f.ex., for (002): F = f$_{Ga}$-f$_{As}$.

16

Al-Ga-N. GaN and AlN have wurtzite (WZ) structure, which is a hexagonal structure, with hcp stacking order but four atoms in the basis instead of two (which hcp has). It is similar to two hcp lattices with a displacement of $[\frac{1}{3}, \frac{1}{3}, \frac{1}{8}]$ relative to each other. The structure factor for GaN and AlN using the position of Ga (Al) and N atoms is:

$$F_{hkl} = \left[f_{Ga} + f_N e^{-\frac{3}{4}i\pi l} \right] \cdot \left[e^{-2\pi i(\frac{1}{3}h + \frac{2}{3}k)} + e^{-2\pi i(\frac{2}{3}h + \frac{1}{3}k + \frac{1}{2}l)} \right] \qquad (2.12)$$

The second term is only kinematically allowed when it is not zero. This formula shows that in WZ structure there are also stronger and weaker reflections, see [Nylund (2018)].

In-Ga-N. The ternary system InGaN has a direct bandgap range from infrared (0.7 eV) to ultraviolet (3.4 eV) [Hsu and Walukiewicz (2008)]. It is therefore an ideal material for solar cells. InN has the same crystal structure as GaN, WZ (hexagonal).

2.4.3 Lattice Defects

In crystals there can be different forms of defects. If there is a change of structure, for example, there is an area of ZB and then there is an area of WZ, in between of those two structures there will be a defect.
Stacking faults is one example of a defect. It characterises a disorder of crystal planes, e.g. ABCABCAB to ABCBACBA.
Twinning is a defect where two crystals share some of the crystal points, see Fig. 2.9b.
For WZ the stacking is ABABAB. If there is a mis-stacking like ABACAB or ABACBCBCB this is called a stacking fault (the ABC close packing is for monoatomic).
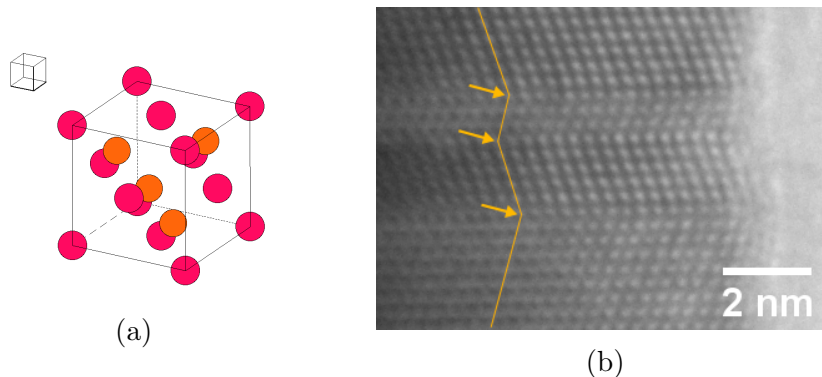
Figure 2.9: (a) Zinc blende structure, made in the software *Vesta*. (b) HRTEM image of a twin in a $GaAs_{1-y}Sb_y$ NW. The arrows point at (111)-twin planes.

2.4.4 NW Applications

NWs could be used in different areas with different implementations. Semiconductor NWs are promising building blocks for optoelectronic devices. The advantage is that different materials can be combined within a single NW and that due to the small diameter, strain can relax on the free surface and NW growth can be on lattice mismatching substrates. Overall less gain material is needed, what is relevant as elements within them are relatively scarce (i.e. expensive) and/or toxic. Beside the examples mentioned in the introduction chapter specifically for III-V NW, other examples relevant for solar cells exist in II-VI systems as for example [Joel and Sehoon (2013)]. However, the field of NW-based devices is compared to thin film technology still young, and research is required both at the synthesis, device design, optimisation and fabrication to realize large scale implementation and to utilise the unique characteristics of such systems fully.

Chapter 3

Experimental Methods

This section describes the sample preparation, the microscopes and software used to collect and analyse the data.

3.1 Material

Several samples with different substrates and elements were used in this study. Tab. 3.1 shows an overview over all the samples used for calibration and mapping. The samples with known thickness and composition were used for calibration of the corresponding ζ-values. These ζ-values were used for mapping to find the samples with unknown thickness and composition. The three systems that were analysed, are Ga-As-Sb, Al-Ga-N and In-Ga-N.

Table 3.1: Samples used for calibration and EDS analysis.

	Sample	ID	System	Details	Comments
A	GaAs	SC-48	Ga-As-Sb	calibration	ζ_{Ga}, ζ_{As}, Shadowing
B	GaAsSb etched	GN-45	Ga-As-Sb	calibration	ζ_{Ga}, ζ_{Sb}
C	GaAsSb	GN-45	Ga-As-Sb		ζ_{Ga}, Shadowing, Mapping
D	GaN/AlGaN	DgFS011	Al-Ga-N	calibration	ζ_{Al}, ζ_{Ga}, ζ_{N}, Mapping
E	GaN/AlGaN	SGN-6	Al-Ga-N		Mapping
F	InAs	NWG-40	In-Ga-N	calibration	ζ_{In}, ζ_{As}
G	InGaN	SGN-8	In-Ga-N		Mapping

3.1.1 Ga-As-Sb

Sample A: GaAs. This sample was previously analysed in [Garmannslund (2016)] by EDS and also in [Kauko et al. (2014)] by HAADF STEM. The NWs were grown with VLS method in a Varian Gen II Modular MBE system by Mazid Munshi. The NWs consist of pure gallium arsenide (GaAs) with ZB structure and growth direction [111] in the bottom part, an axial GaAsSb insert and pure GaAs with WZ structure and [0001] growth direction in the top part. The substrate is Si(111).

In this thesis the sample is used as reference for ζ_{Ga} and ζ_{As}, and for analysing the shadowing of the sample holder. Growth specifications are listed in Tab. 3.2.

Table 3.2: GaAs reference sample grown at $T_c = 620$ ^{o}C.

	element	flux [Ml/s] monolayer per second	duration
1.	Ga	0.7 Ml/s	20 min
	As	4.2E-6 Torr	
2.	Ga	0.7 Ml/s = 3.3E-7 Torr	1 min
	As	4.2E-6 Torr	
	Sb	1.1E-6 Torr	
3.	Ga	0.7 Ml/s	5 min
	As	4.2E-6 Torr	

Sample B: GaAsSb. For sample B, the NWs were grown on graphene glass by Dingding Ren at the Department of Electronic Systems at NTNU, Trondheim, by using VLS epitaxy. A graphene layer on top of SiO_X, described in [Sun et al. (2015)], was used as substrate. Here a 10 x 10 mm piece was cut out and inserted into an MBE machine. In UHV, the sample was heated to 625°C. Then, Al in vapour phase was directed onto the sample and deposited for one second with a flux of 0.1 monolayers per second. On the substrate the Al forms liquid islands. After that, the Al beam was closed and the As_2 and Sb_2 beam opened for 1 min to allow As and Sb to dissolve into the Al islands to form $AlGa_{x-1}As_x$ as seed particles to start the growth. Then, the As and Sb beam is closed and the Ga beam opened for 5 s. During that time Ga droplets form. The last step is to have the Ga, As and Sb beam directed onto the sample. This deposition phase lasts for 10 min. In that time, the NW grows. The crystal is growing at the point where the liquid

Ga droplet meets the NW crystal (or seed particle in the beginning) and the vapour phase around it. The Ga droplet stays on top of the NW and the NW is growing underneath the droplet as long as Ga is fed into the droplet and Sb and As fluxes directed onto the sample. Table 3.3 lists the growth parameters.

Table 3.3: Specifications during MBE growth, the whole process happened at $T_c = 625^oC$.

	element	flux [Ml/s] monolayer per second	duration
1.	Al	0.1	1 s
2.	As$_2$	2.5E-6	1 min
	Sb$_2$	6E-7	
3.	Ga	0.7	5 s
4.	Ga	0.7	10 min
	Sb	2.5E-6	
	As	2E-7	

Sample C: GaAsSb etched. A part of sample B was taken and etched to get sample C. This etching process, one minute immersion in hydrochloric acid fuming 37 %, should remove the Ga droplets from the NWs and parasitic crystals. This etched sample was examined with the SEM and TEM for the first time in this thesis.

3.1.2 Al-Ga-N

Sample D: GaN/AlGaN. This sample was MBE grown at Tokyo University by Andreas Liudi Mulyo. It is an AlN/GaN/n-AlGaN/AlN/p-AlGaN/GaN grown on graphene on fused silica.
The fused silica, AlN, GaN bottom and top and the protection layer electron deposited C was used to find ζ-values and the n-AlGaN/AlN/p-AlGaN as heterostructure to map.

Sample E: GaN/AlGaN. This sample was grown with MBE by Dingding Ren and the substrate was graphene glass. First, AlN nucleation particles were grown, then GaN NWs grew on top of the seed particles. Growth pa-

rameters are given in Tab. 3.4. Previous characterisation work on this sample can be found in Nylund (2018).

Table 3.4: Specifications during MBE growth of sample E.

element		Temperature T_c [^{o}C]	flux [Ml/s] monolayer per second	duration
1.	Al	600	0.1	400 s
	N_2		2.7/480 sscm/W	
2.	Ga	960	0.3	4 hrs
	N_2		2.7/480 sscm/W	

3.1.3   In-Ga-N

Sample F: InAs. The InAs sample, which was used here as reference, was grown in the MBE on kish-graphite substrate by Mazid Munshi. GaAs was grown at 450 ^{o}C for 45 min. Tab. 3.5 shows growth parameters.

Table 3.5: Specifications during MBE growth of sample F.

element		Temperature T_c [^{o}C]	flux [Ml/s] monolayer per second	duration
1.	Ga	450	0.1 (=0.2 Å/s)	45 min
	As_4		$3 \cdot 10^{-6}$ Torr	

Sample G: InGaN. This sample was grown by Dingding Ren in the MBE. The substrate is graphene glass fabricated at Peking University. The NWs consist of n-type AlN with Si dopant 1100, n-type GaN with Si dopant 1100 and intrinsic InGaN.

Table 3.6: Specifications during MBE growth of sample G.

	element	Temperature T_c [^{o}C]	flux [Ml/s] monolayer per second	duration
1.	Al	600	0.1	400 s
	N_2		2.7/480 sscm/W	
2.	Ga	960	0.3	3 hrs
	N_2		2.7/480 sscm/W	
3.	In	620	0.2	1 hrs
	Ga		0.1	
	N_2		2.7/480 sscm/W	

3.2 Electron Microscopy

For this thesis the SEM FEI-Apreo located in the cleanroom Nanolab, and the TEM JEOL JEM-2100 were used. Voltages in the SEM ranged between two up to 20 kV. The TEM was used with an acceleration voltage of 200 kV. The TEM sample holder was a double tilt beryllium holder. The light Beryllium minimises the background signal, which is especially important in the EDS analysis. The condensor lens aperture in the TEM had a diameter of 40 μm if not stated otherwise. For HAADF STEM images in the TEM, the ADF detector was used at a camera length of 12 cm, corresponding to an inner ADF detector angle of approximately 50 mrad. For acquiring EDS data, an Oxford X-Max 80 SDD detector was used. The detector has an energy resolution of approximately 130 eV. All EDS was measured in STEM mode while the detector was operated by AZtecEnergy software.

To be able to study a sample with TEM or SEM, it has to be prepared prior to inserting it into the microscope.

3.2.1 SEM sample preparation

For the SEM the samples could be used directly after the NWs were grown onto the substrates in the MBE machine.

3.2.2 TEM sample preparation

For the TEM, the sample had to be prepared further. The following steps were taken for the GaAsSb sample (Sample B and C); The sample for the

SEM was scratched with a diamond scratcher. Fig. 3.1 shows an SEM image of the scratches, which can be seen as dark lines. As a TEM grid, a holey C-film on 300 mesh Cu grid was taken and swiped over the sample to deposit some of the scratched off parts of the sample onto the grid.

The FIB sample was made by Per Erik Vullum at an FEI Helios. A FIB sample was used to have a constant thickness and that the electron beam should go through one crystal with a constant composition (sliced by FIB). The thickness was estimated by t/λ in EELS. This thickness interface area is about 140 nm.
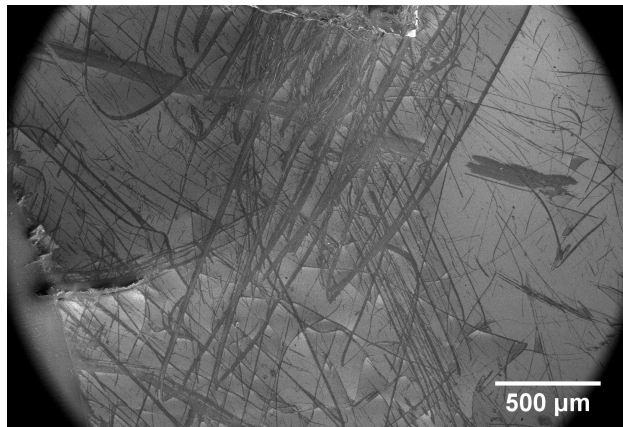
Figure 3.1: SEM overview of the GaAsSb sample, ETD 2 kV.

For the samples InAs and InGaN, samples F and G, the preparation had one additional step. (The same had been done for GaN/AlGaN, sample E.) A drop of isopropanol was deposited onto the scratched substrate with a pipette. The 300 mesh Cu grid was then swiped over the isopropanol droplet with NW in it. The isopropanol evaporated leaving scratched off particles including NWs on the grid.

Fig. 3.2 shows an area of the GaAsSb sample B (left) and of the GaN/AlGaN sample E (right) in the TEM. Apart from different NWs, many of the parasitic crystals can be seen in the GaAsSb sample. The parasitic crystals are too thick for electrons to pass through and cannot be analysed further with a TEM.
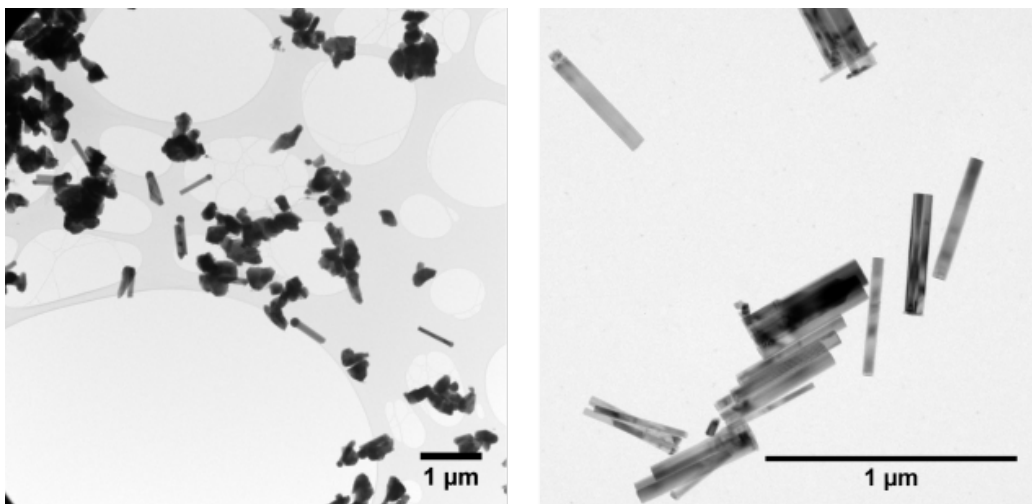
Figure 3.2: Lower magnification of part of the GaAsSb TEM sample.

3.3   Data Analysis

Image processing was done using the softwares *Digital Micrograph* and *ImageJ. Python* was used for further data processing including spectrum images using the Hyperspy library. The code is given in Appendix D.

The .oip maps from AZtek were converted to .hdf5 files using the Hyper-Spy Script from Adrian Lervik. This script uses for each conversion a .msa spectrum for energy calibration, a .raw and .rpl file for map data and a .txt file for spatial calibration data. If not specified otherwise, for ζ-calibration the data was binned and fitted to a model. For mapping, PCA was used to maintain a high spatial resolution and then fitted to a model. Functions written by Andreas Garmannslund were used to create compositional and thickness maps. The k-factors for the CL-method were used from the AZtek software.

Chapter 4

Results

In this section, the results of the three systems Ga-As-Sb, Al-Ga-N and In-Ga-N are presented.

4.1   Electron dose

For the zeta calibration, the electron dose was measured using the CCD camera. With the constant 4.855 by [Nylund (2018)], the counts on the CCD can be related to the number of electrons on the sample. For different spot sizes and CL apertures, the beam current changes. There are four different CL apertures in the microscope, 10, 40, 100 and 200 μm. From the spotsizes, 0.7, 1 and 1.5 nm were chosen. With a bigger CL, more electrons hit the sample. Using a bigger spotsize, also more electrons hit the sample, see Fig. 4.1.

For EDS measurements, spot sizes of 0.7 nm and 1 nm were chosen. For all measurements, the 40 μm CL aperture was used. This leads to currents of 0.2 nA to 0.4 nA, see Tab. 4.1.

Table 4.1: Electron dose averaged.

Spotsize diameter [nm]	0.7	1	1.5	2
Probe current [nA]	0.2	0.4	1	1.75
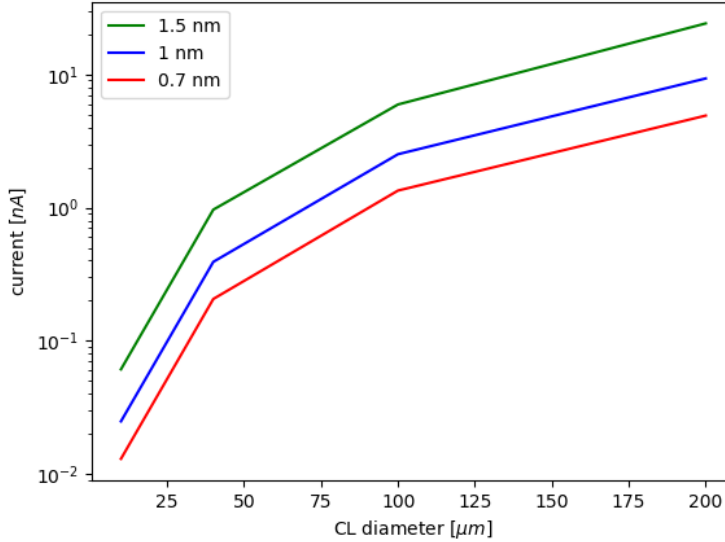
Figure 4.1: Probe current vs. condensor aperture size for three different spot sizes: 0.7 nm, 1 nm and 1.5 nm.

4.2 Shadowing

The holder can be tilted towards or away from the EDS detector. If the holder is tilted away from the detector, the holder is shadowing the detector and a lower signal gets to the detector. This increases the zeta value. Fig. 4.2 shows a tilt series of a Ga droplet of sample C, GaAsSb, in black. There is also a tilt series from the Ga droplet of sample A, the GaAs reference sample, and from the Ga and As from the NW of that GaAs reference sample. The analysed NW including the map areas are shown in Figure Fig. 4.2 on the left.

It can be seen that the zeta values for Ga and As are quite constant between 0° and 35° tilt. Below 0° the ζ-values increase. The zeta values of Ga in the droplets is in the same range of both samples (black: 1823 $\pm$3% and green: 1756 $\pm$7%). It can be noted that ζ_{Ga} from the droplets is consistently higher than ζ_{Ga} from the NW.
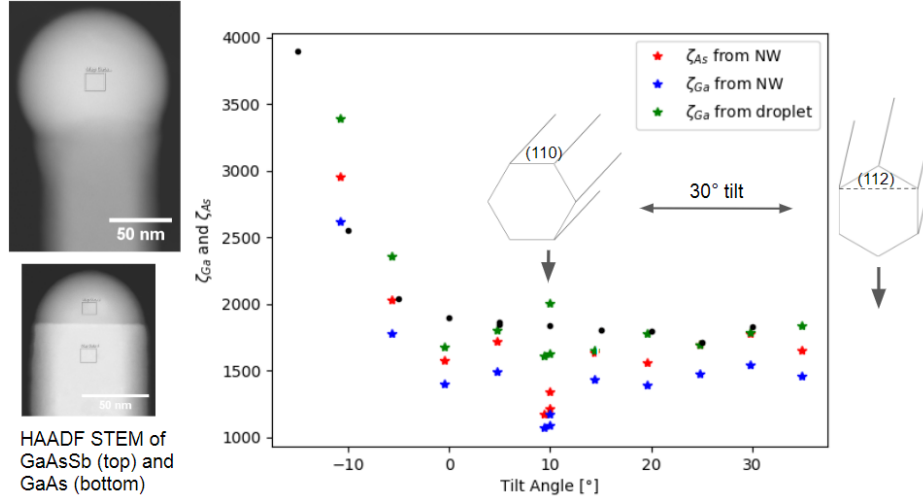
Figure 4.2: Tilt series of the Ga droplet of sample C, a GaAsSb NW (top left) and sample A, a GaAs NW (bottom left). The black measurement points are from sample C, the blue, red and green from sample A. The black and the green are from NW droplet, the red and blue from a NW.

4.3 Reference Samples GaAs, AlGaN, InAs

For the zeta calibration, reference samples of known composition and thickness were used.

GaAs NWs, sample A, were available for calibration of ζ_{Ga} and ζ_{As}. Fig. 4.3 shows a BF image of a typical NW (a), HR images of the top part (b) and the middle (c), and HAADF STEM images of the NW (d), the top (e) and the middle (f). Calibration maps were taken in the middle of the NW.

A reference sample to determine ζ_{Sb} is sample B, GaAsSb etched. This is the GaAsSb sample (sample C), but the Ga etched away. Removing the droplet is also a way to proof that the top crystal is GaSb. Fig. 4.4 shows an SEM image of the top view of the sample (a), a BFTEM images (b) with SAED patterns of the top (c) and middle (d) part of the NW. A HRTEM image (e) shows the top crystal and a HAADF STEM image shows the whole NW (g) and the top part of the NW (f). In the SEM image the hexagonal cross-section of the NWs can be seen as the Ga droplets are not covering them
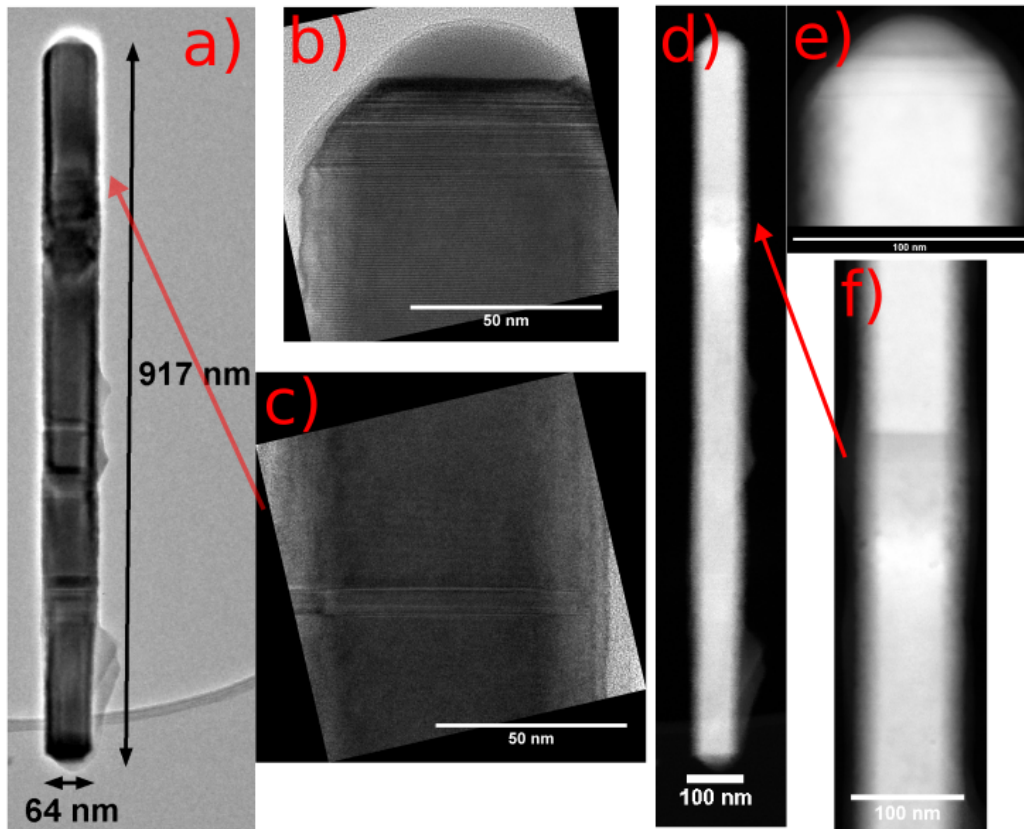
Figure 4.3: GaAs reference sample, sample A. BFTEM (a), HRTEM (b and c) and HAADF STEM images (d, e and f) are shown.

anymore. Also the polycrystaline crystals have no more droplets on them. The HRTEM images shows carbonious contamination around the top crystal.

The GaN reference sample, sample D, was a FIB lamella. It was mounted onto a half grid. Fig. 4.5 shows the lamella (a) where the grid can be seen on the sides as dark area, and the NW which were used for EDS analysis (b). The thickness was analysed using EELS data by Per Erik Vullum.

InAs, sample F, was the reference sample for calibration of ζ_{In} and ζ_{As}. The NWs were a little asymmetric which makes the thickness estimation difficult. EDS maps were taken in the middle of the NW where the NW was assumed to be symmetric. Fig. 4.6 shows a HRTEM image (a), a SAED
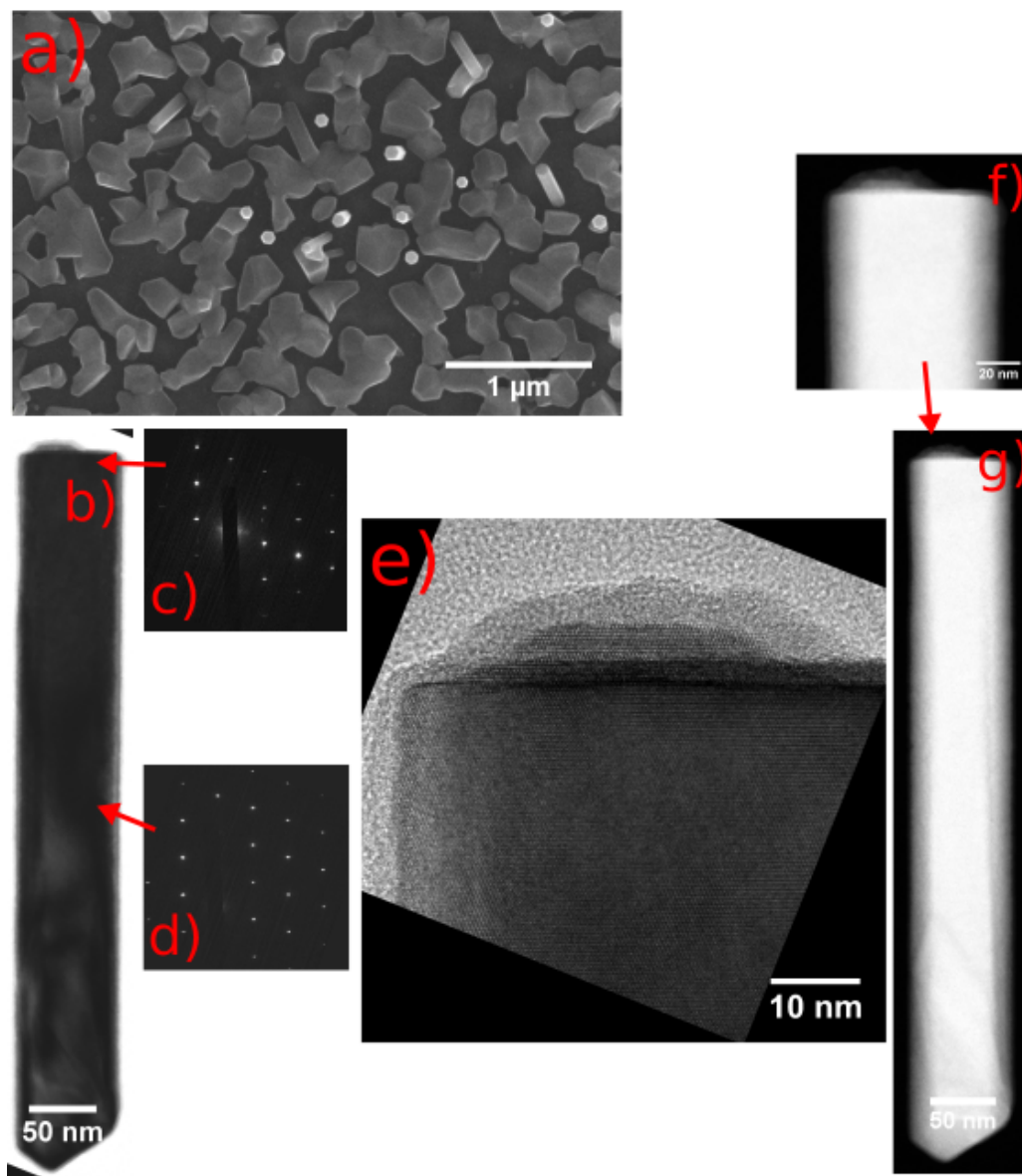
Figure 4.4: GaAsSb etched reference sample, sample B. The Ga droplets were removed. A SEM image (a), a BFTEM (b), SAED of top (c) and middle (d) are shown. A HRTEM image (e) shows carbonious contamination around the top crystal. HAADF STEM images of the NW (g) and the top of the NW (f) show the same NW.
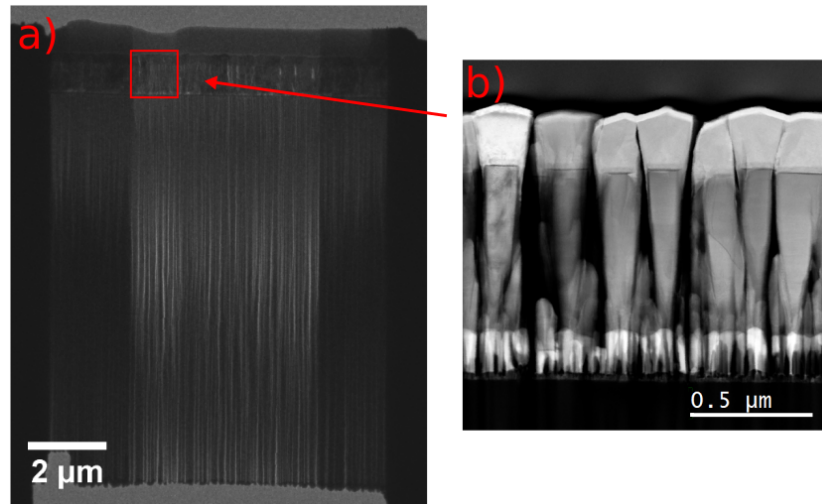
Figure 4.5: GaN/AlGaN reference sample, sample D. An overview shows the FIB lamella (A) and a HAADF STEM images (b) shows the analysed area.

image (b) and a HAADF STEM image (c) of a NW used for EDS. There are several stacking defaults, which can be seen in the HRTEM image. In the SAED image, the defects are visible as they smear out the diffraction spots to lines. The HAADF STEM image (c) shows the whole NW. The asymmetry can be seen in the top part. At the bottom right part of the NW there is an overlapping particle.
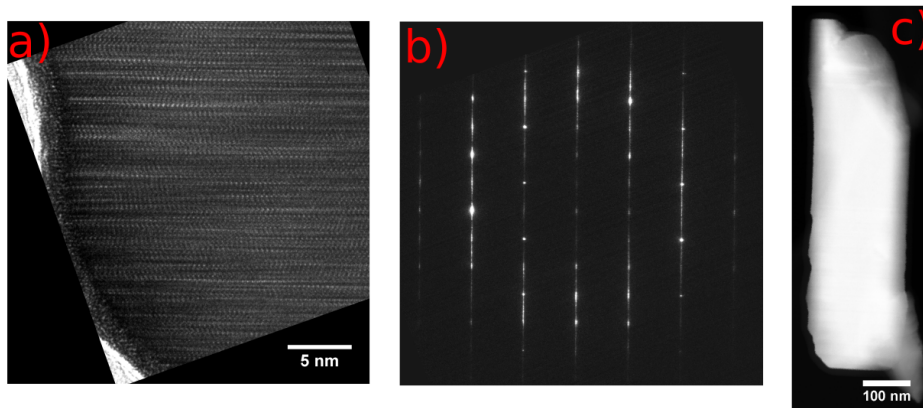
Figure 4.6: InAs reference sample, sample F. A HRTEM image (a), SAED image (b) and HAADF STEM image (c) are shown.

31

4.4 Zeta constant of elements

The zeta values of the K-lines and L-lines of the elements is plotted against the transition energies of the elements, see Fig. 4.7. The error is the error is not indicated in this plot, but from the measurements depicted in Fig. 4.2 it is rather large.
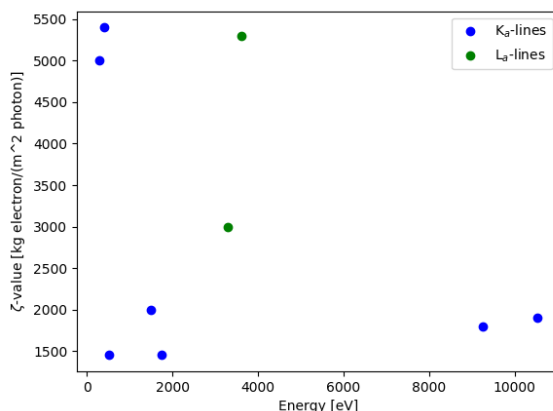
Figure 4.7: Zeta values of K-lines and L-lines for JEOL JEM2100F of the elements analysed.

4.5 Samples Ga-As-Sb, Al-Ga-N, In-Ga-N

GaAsSb, sample C, has straight NWs and NWs grown at an angle. There is an Sb-rich crystal at the top. The NWs are almost defect free apart from some twinning defects at the bottom. In addition to the NW growth, there was a high number of polycrystalline 2D growth crystals.

Fig. 4.8 shows SEM images of the same area of the GaAsSb sample, sample C, in 45 ^{o}tilted (a) and top view (b). The orange rectangle in both SEM images shows the same NW. In the tilted view, the NW and the droplet can be seen, in the top view only the round droplet is visible. Fig. 4.8 also shows a BFTEM image of one NW (c), a SAED image (d) from the middle of the NW and the HRTEM image of the same NW (e). This NW probably grew at an angle since it has a bend at the bottom edge. The SAED image

shows the ZB structure and the HRTEM image presents the GaSb top crystal.
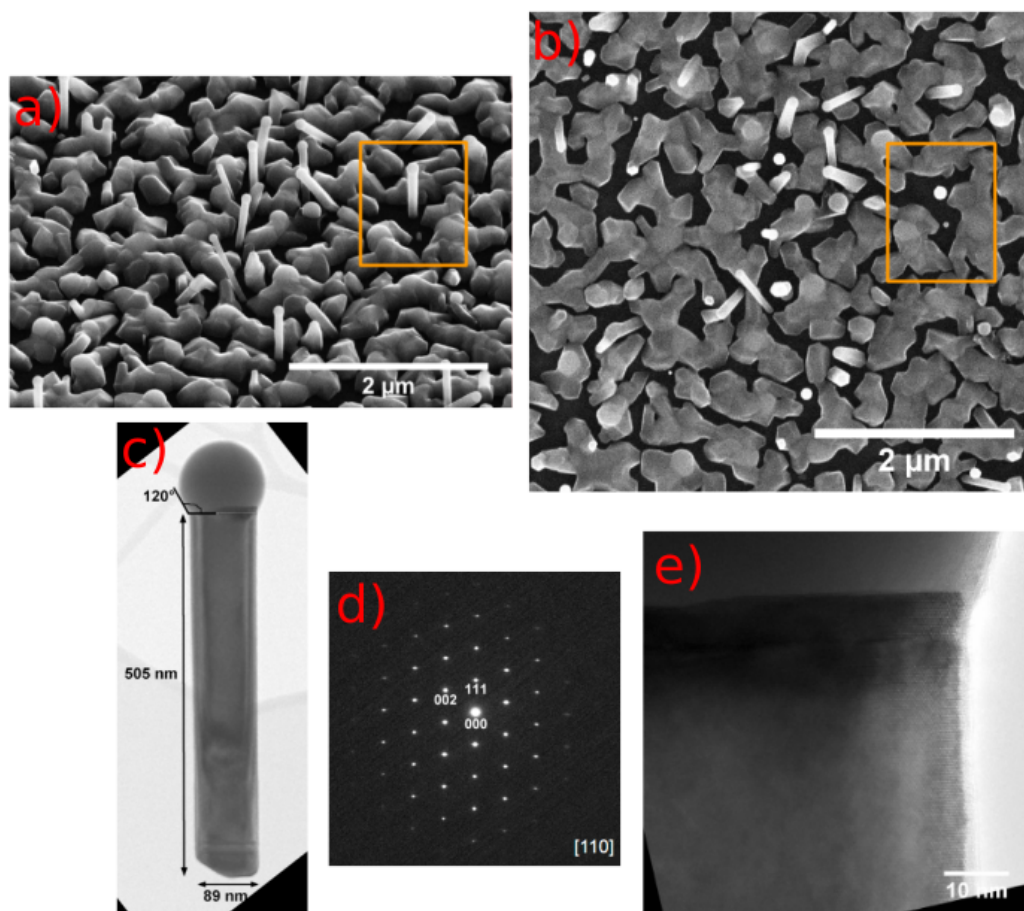
Figure 4.8: GaAsSb sample, sample C. SEM images (a and b) of the same area, a BFTEM (c), SAED (d) and HRTEM image (e) are shown. The orange rectangle points to the same NW.

AlGaN/GaN, sample E, was used for elemental mapping. The bottom part of one NW was used for EDS analysis. Fig. 4.9 shows the BF image (a) of two NWs. The right one of the two NWs is used for analysis and EDS mapping. The bottom part is shown in the HRTEM image (b). A SAED image (c) and a HAADF STEM image (d) are shown. The SAED image shows the WZ crystal structure. Diffraction spots of different intensities can be seen as mentioned in the theory chapter. The HAADF STEM image was taken after tilting the NW on zone, before the EDS data were taken. By focusing the electron beam onto the NW, it damaged the NW. This damage can be seen as a dark spot in the HAADF STEM image (d), the red arrow is pointing at it. That means that the AlGaN/GaN NWs have a lower maximum electron dose than the NW from samples A - C as these samples had no visible damage.
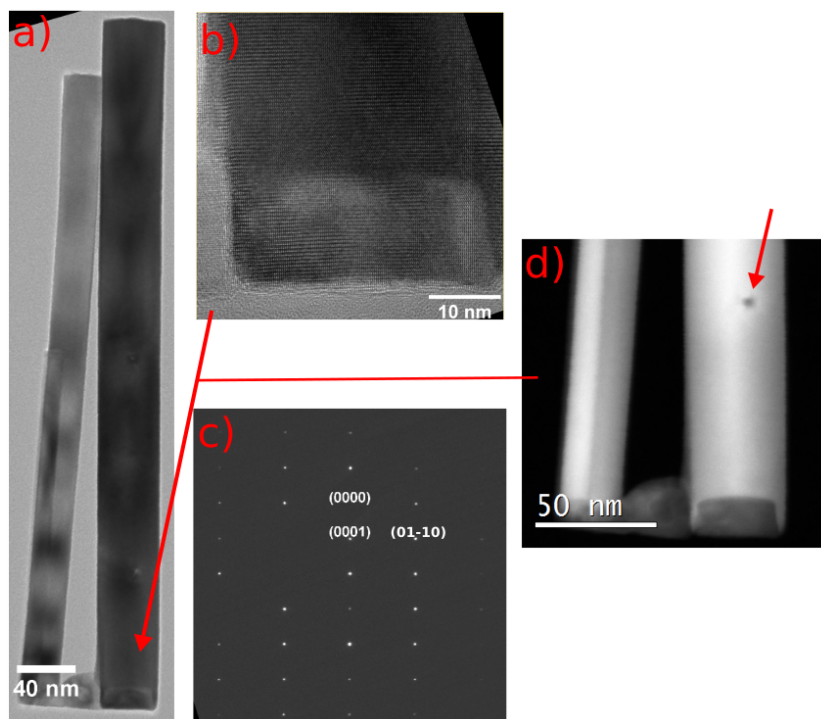
Figure 4.9: AlGaN/GaN sample, sample E. A BFTEM image (a), HRTEM (b), SAED image (c) and a HAADF STEM image (d) are shown. The dark spot in (d) is damage by the electron beam.

InGaN is a new sample, sample G, which is analysed here for the first time. Fig. 4.10 shows SEM images in top view (a) and 45° tilt (b). The hexagonal shape of the top part of the NWs can be seen. The NWs vary a lot in size. The NW density is very high, that is why the NWs were usually seen in clusters on the TEM grid. One NW was chosen for EDS analysis. A BFTEM (c), HRTEM (d), SAED (e) and HAADF STEM image (f) is shown. In the BFTEM and HAADF STEM image there is an overlying particle at the bottom of the NW.
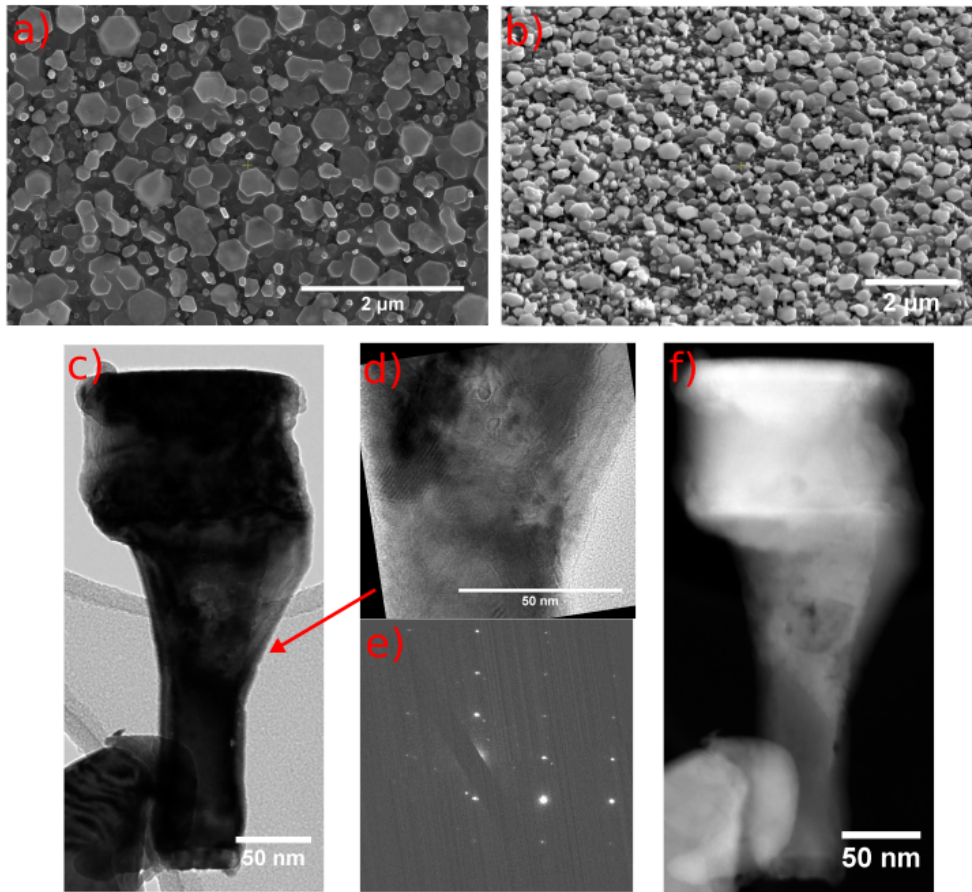
Figure 4.10: InGaN sample, sample G. SEM images of top view at 20 kV (a) and 45° tilt at 10 kV (b). A BFTEM (c), HRTEM (d), SAED (e) and HAADF STEM image (f) are shown.

4.6 Elemental composition of the three systems

In this section, the composition of the three systems is analysed using elemental maps and thickness maps while comparing the CL-method to the ζ-method. Non-negative matrix factorisation (NMF), was used before calculating the CL- and ζ-quantification maps.

4.6.1 Ga-As-Sb

System 1 is GaAsSb, sample C. The composition and thickness of the top crystal is analysed in Fig. 4.11. The left image shows the map area, the right image shows the thickness of that area in arbitrary units.
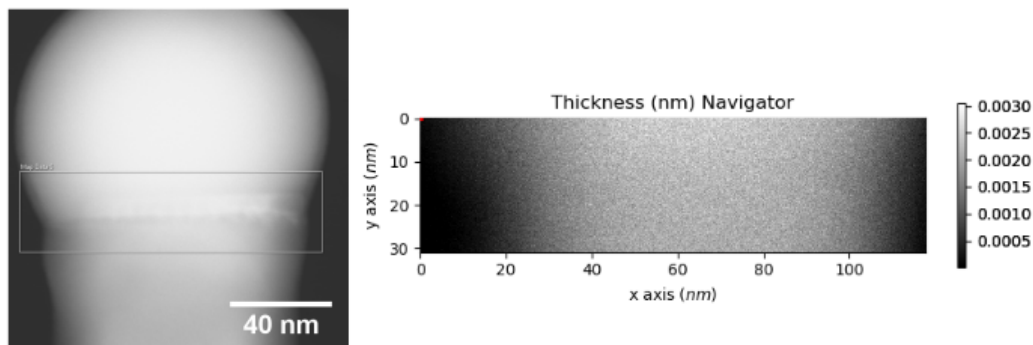
Figure 4.11: Map area of the top part of a NW of sample C, GaAsSb, (left) and a thickness map with arbitrary units (right).

Fig. 4.12 shows maps of atomic percentages of Ga, As and Sb for Zeta quantification (left column) and CL (right column). Note: the scales of the two methods is different for each element.
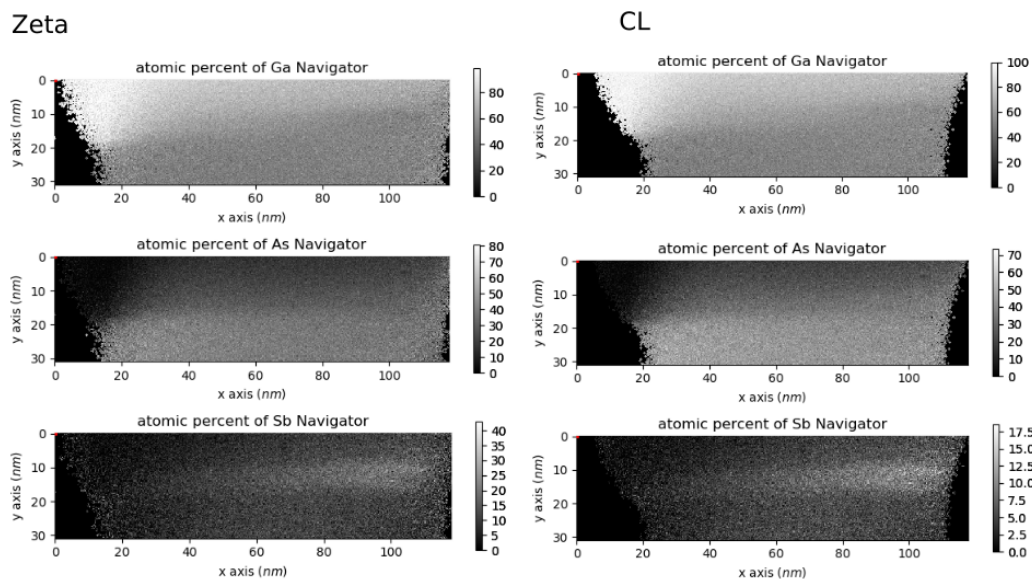
Figure 4.12: Comparison of the Zeta method to the CL method of a NW of sample C. PCA with additional constraint of non-negative matrix factorisation (NMF) is used and no binning.

4.6.2 Al-Ga-N

System 2 is AlGaN/GaN, sample E. The composition at the bottom end of the NW and the composition and thickness of the seed particle is analysed here. Fig. 4.13 shows the map area (left) and a thickness map with arbitrary unit (right). In the left image, damage can be seen in the bottom of the NW at the seed particle. This damage originated from previous EDS analysis that measuring day.

Fig. 4.14 shows the maps of atomic percentages of Al, Ga and N for Zeta quantification (left column) and CL (right column). Note: the scales of the two methods is different for each element.
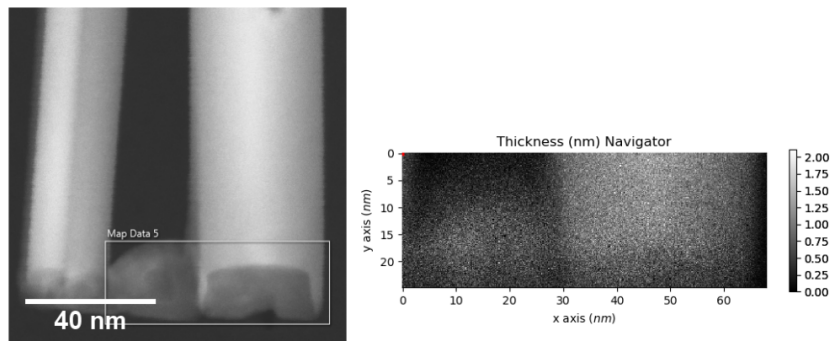
Figure 4.13: Map area of the bottom part of a NW of sample E, AlGaN/GaN, (left) and a thickness map with arbitrary units (right).
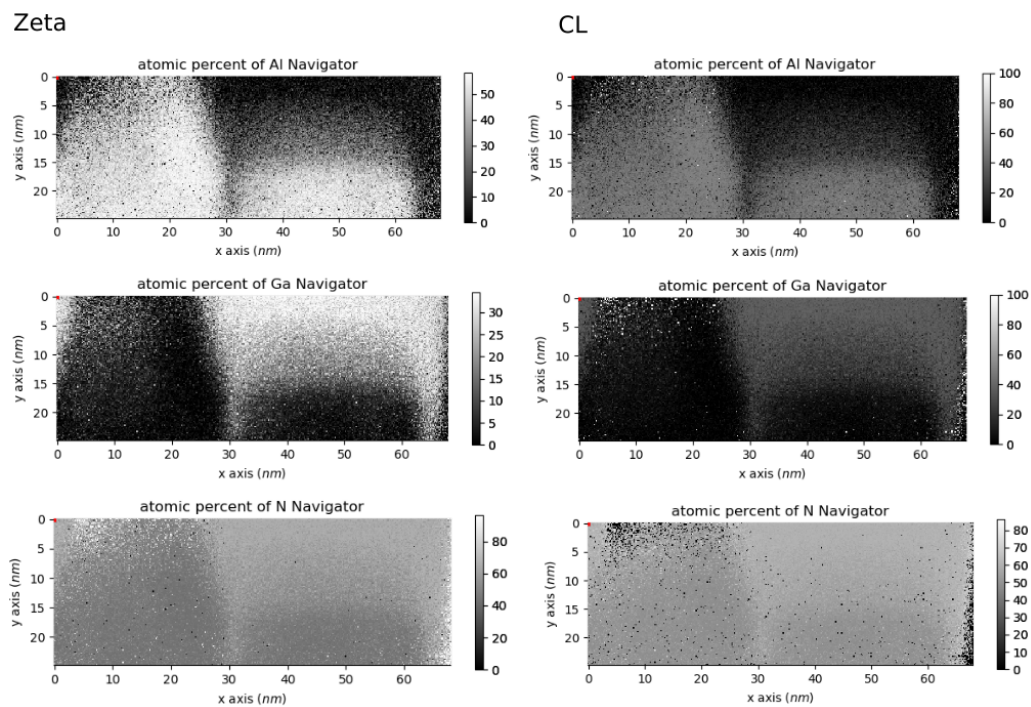
Figure 4.14: Comparison of the Zeta method to the CL method of a NW of sample E. PCA with additional constraint of non-negative matrix factorisation (NMF) is used and no binning.

4.6.3   In-Ga-N

System 3 is InGaN, sample G. The composition and thickness of the top part of the NW is analysed here. Fig. 4.15 shows the map area (left) and a thickness map with arbitrary unit (right).
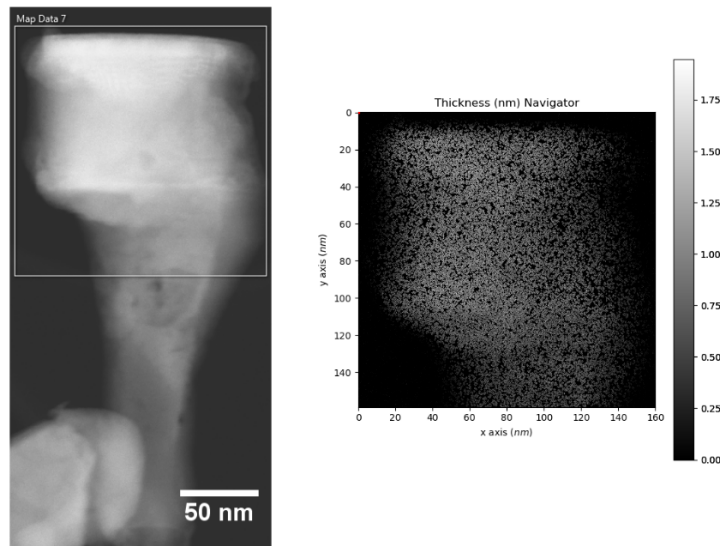
Figure 4.15: Map area of a NW of sample G, InGaN, (left) and a thickness map with arbitrary units (right).

4.16 shows the maps of atomic percentages of In, Ga and N for Zeta quantification (left column) and CL (right column). The CL method does not show many data points here.
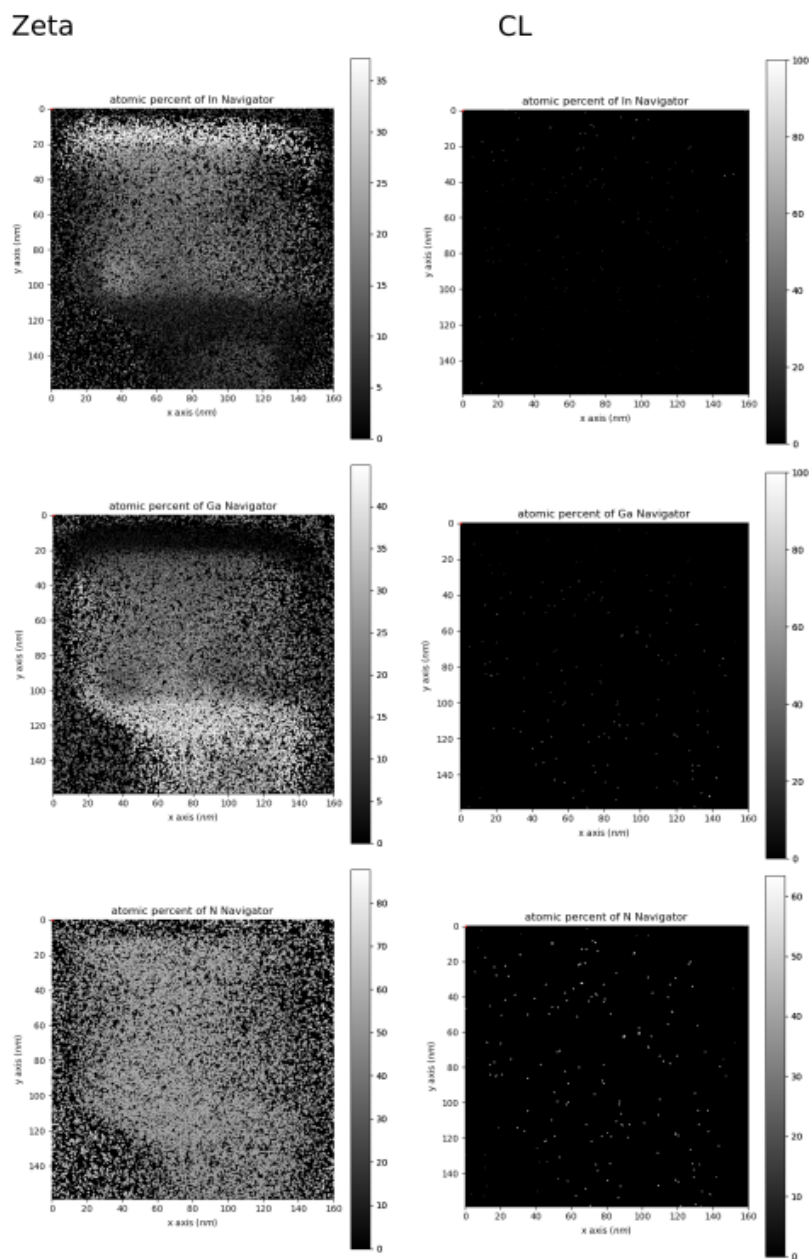
Figure 4.16: Comparison of the Zeta method to the CL method of a NW of sample G. PCA with additional constraint of non-negative matrix factorisation (NMF) is used and no binning.

Chapter 5

Discussion

The CL aperture and spotsize were chosen depending on the sample analysed. This was done to have adjust the number of electrons hitting the sample. The more electrons hit the sample, the more counts can be detected with the EDS detector and thus give a better signal. But if there are too many electrons on the sample, the sample gets damaged. The ideal case is to have the maximum possible number of electrons without damaging the sample. This number changes from sample to sample because thinner lighter samples are damaged more easily. Here it is the sample with the light elements N and Al in sample D and E.

Zeta Ga values are consistently higher in the droplet than in the NW. This might be due to thickness over- or underestimation. The droplet could be not perfectly spherical but due to gravity slightly elliptical. The NW could also be asymmetrical. There could be other elements, contaminations, on the droplet which are not assumed to be there.

The ζ-values are calculated. Several factors influence the error of the ζ-values. The raw signal has noise. This is always there but can be reduced with binning or methods such as PCA. The electron dose is an estimation, which has an error. Measuring the electron dose can reduce this error. The error of the ζ-values are also dependend on an error in sample thickness and on the error in the reference sample composition.
The estimated ζ-values have a very large error. It is therefore difficult to find a relation between the values of the K- and L-lines and the x-ray transition energies, which was f.ex. done in [Garmannslund (2016)] with the TEM

JEOL ARM200F.

All three sample classes analysed here have their difficulties. The first system, $GaAs_{1-y}Sb_y$, has a crystal embedded in the Ga droplet with an unknown shape. The second system has N_K (0.39 eV absorbed), and a seed crystal AlN embedded in the GaN NW. The third system has extreme thickness variations affecting quantification.

In system two, AlGaN/GaN, damage is a problem. Fig. 5.1 shows a HRTEM image before (top image) and after (bottom image) an EDS scan. The electron beam damaged the bottom of the NW and a hole formed. If the beam current is smaller, the EDS signal is weaker. For good maps, though, the count rate should always be bigger than 1000 counts per s.
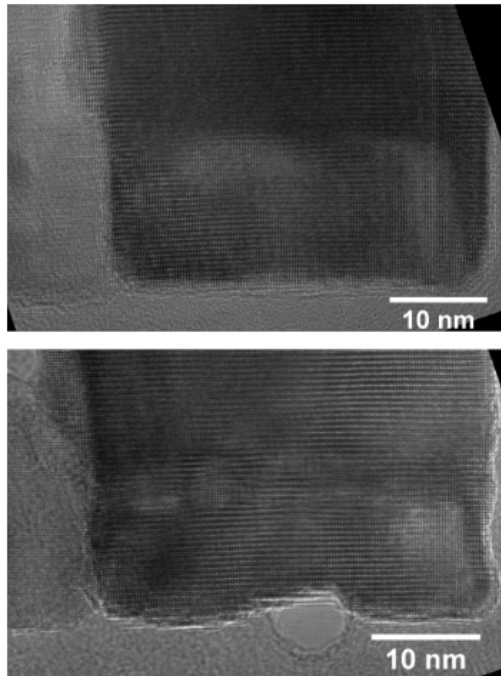
Figure 5.1: Limitation to beam damage. The top image was taken before EDS scan, the bottom image after the scan.

Chapter 6

Conclusion

In this project the ζ-method was for the first time set-up on the TEM-EDS system used in this study. This included 1) to convert data from other software format, recalibrate and save appropriately in .hdf5. 2) get ζ-factors calibrated for different relevant elements testing different specimen geometries, structures, condensor and holder tilt settings and 3) do all data processing within HyperSpy notebook which is transparent and transferable to co-workers and can include more advanced data processing routines such as PCA-based denoising and NMF blind source separation. The developed approach was applied to some example heterostructures of interest to NW-based optoelectrical devices.

Chapter 7

Further Work

As next step, the ζ calibration can be improved. More reference samples are needed to get better statistics. Also, the dose measurements can be more precise. The current can be directly measured in the TEM with an ammeter to improve the previously determined constant between the current on the sample and the current on the CCD camera.

The estimated ζ-values have an error range. This error range can be calculated more precisely.

The absorption correction can be included in the ζ method. This would improve the accuracy of the light elements such as nitrogen.

The InGaN/GaN FIB sample, sample D had one interface layer. The composition of this interface can be analysed.

The GaSb top crystal in sample B can be analysed in more detail. Up to now this sample was used for ζ-calibration, but the geometry of the crystal can be analysed further.

Bibliography

Bearden, J. A. (1967). X-Ray Wavelengths. *Reviews of Modern Physics*, 39:78–124.

Cliff, G. and Lorimer, G. W. (1975). The quantitative analysis of thin specimens. *Journal of Microscopy*, 103(2):203–207.

Edington, J. W. (1976). *Typical Electron Microscope Investigations*, pages 1–112. Macmillan Education UK, London.

Garmannslund, A. (2016). Refinement of the ζ-factor method for quantitative energy-dispersive x-ray spectroscopy in scanning transmission electron microscopy. .

Goldstein, J., Goldstein, J., Goldshtain, Y., Newbury, D., Joy, D., Echlin, P., Lyman, C., Lifshin, E., Sawyer, L., Joy, O., et al. (2003). *Scanning Electron Microscopy and X-ray Microanalysis: Third Edition*. Scanning Electron Microscopy and X-ray Microanalysis. Springer US.

Hsu, L. and Walukiewicz, W. (2008). Modeling of ingan/si tandem solar cells. *Journal of Applied Physics*, 104(2):024507.

Jany, B. R., Janas, A., and Krok, F. (2017). Retrieving the quantitative chemical information at nanoscale from scanning electron microscope energy dispersive x-ray measurements by machine learning. *Nano Letters*, 17(11):6520–6525. PMID: 29032683.

Joel, J. and Sehoon, C. (2013). Zno nanowire arrays for enhanced photocurrent in pbs quantum dot solar cells. *Advanced Materials*, 25(20):2790–2796.

Kauko, H., Fimland, B. O., Grieb, T., Munshi, A. M., Müller, K., Rosenauer, A., and van Helvoort, A. T. J. (2014). Near-surface depletion of antimony

during the growth of gaassb and gaas/gaassb nanowires. *Journal of Applied Physics*, 116(14):144303.

Krogstrup, P., Ingerslev Jørgensen, H., Heiss, M., Demichel, O., Holm, J., Aagesen, M., Nygard, J., and Fontcuberta i Morral, A. (2013). Single nanowire solar cells beyond the shockley-queisser limit. ., 7.

Nylund, I.-E. (2018). Electron microscopy characterization of iii-nitride nanowires grown on graphene. *Master Thesis*.

Otnes, G. and Borgström, M. T. (2017). Towards high efficiency nanowire solar cells. *Nano Today*, 12(Supplement C):31 – 45.

Papadopoulos, C. (2014). *Solid-State Electronic Devices: An Introduction.* Undergraduate Lecture Notes in Physics. Springer New York, New York, NY.

Sun, J., Chen, Y., Priydarshi, M. K., Chen, Z., Bachmatiuk, A., Zou, Z., Chen, Z., Song, X., Gao, Y., Rümmeli, M. H., Zhang, Y., and Liu, Z. (2015). Direct chemical vapor deposition-derived graphene glasses targeting wide ranged applications. *Nano Letters*, 15(9):5846–5854. PMID: 26305883.

Wagner, R. S. and Ellis, W. C. (1964). Vapor-liquid-solid mechanism of single crystal growth. *Applied Physics Letters*, 4(5):89–90.

Watanabe, M. and Williams, D. B. (2006). The quantitative analysis of thin specimens: a review of progress from the cliff-lorimer to the new ζ-factor methods. *Journal of Microscopy*, 221(2):89–109.

Williams, D. and Carter, C. (2009). *Transmission Electron Microscopy: A Textbook for Materials Science.* Number v. 2 in Cambridge library collection. Springer.

Appendix A

Energy bandgap

In Fig. A.1 the energy bandgap is plotted against the lattice constant. The lattice constant for GaAs is just above 5.6 Å, whereas pure GaSb has a lattice constant of 6.1 Å. That is why changes in composition of GaAs$_{1-y}$Sb$_y$ can be seen as a change in the lattice constant. Comparing GaAs and AlAs, the difference in lattice constant is too small to see in a TEM image using FFT. Thus, if there is a crystal in the bottom part of a NW, which consists of more Al than Ga, it could not be seen in BF-TEM or HRTEM.
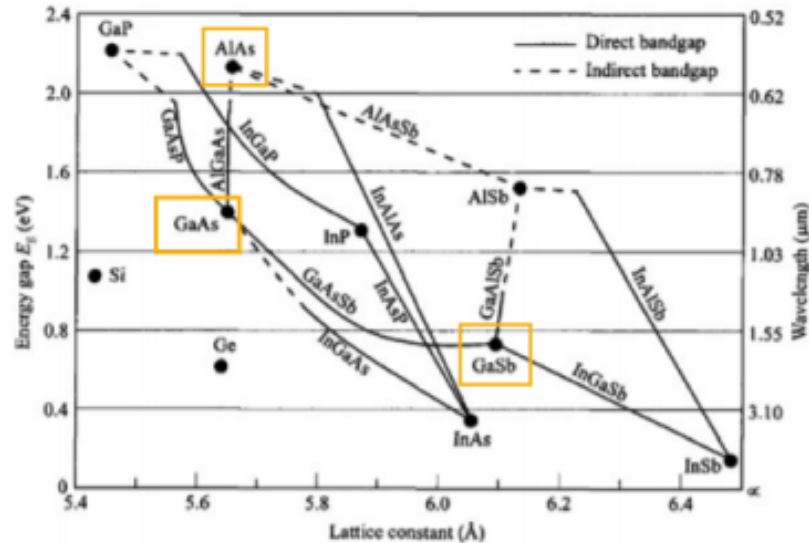
Figure A.1: Lattice constant vs. energy bandgap [Papadopoulos (2014)].
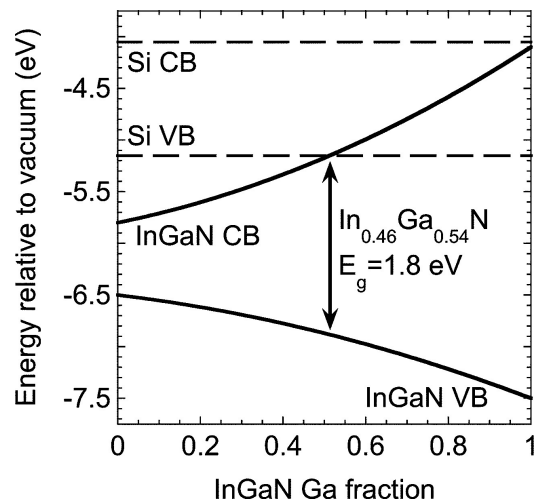
Figure A.2: The energy bandgap changes depending on the composition of InGaN [Hsu and Walukiewicz (2008)].

For InGaN, the bandgap ranges from 0.7 to 3.4 [Hsu and Walukiewicz (2008)], see Fig. A.2.

Appendix B

K and L X-ray line transition energies

Detected energies of X-ray emission lines in the EDX analysis are listed in Tab. B.1. Elements of group III are Al, Ga and In, elements of group V are N, As and Sb. C, O and Si are part of the substrates.

Figure B.1: Elements of interest, silicon, carbon and oxide are found in the sample substrates.

Table B.1: Main transition energies in eV for C, O, Si, Cu, Ga, As and Sb [Bearden (1967)].

Element	$K\alpha_1$	$K\alpha_2$	$K\beta_1$	$L\alpha_1$	$L\alpha_2$	$L\beta_1$	$L\beta_2$	L_ℓ
6 C	277							
7 N	392.4							
8 O	524.9							
13 Al	1,486.7	1,486.3	1,557.4					
14 Si	1,739.98	1,739.38	1,835.9					
29 Cu	8,047.78	8,027.8	8,905.3	929.7		949.8		811.1
31 Ga	9,251.74	9,224.8	10,264.2	1,097.92	1,097.92	1,124.8		957.2
33 As	10,543.72	10,508.0	11,726.2	1,282.0	1,282.0	1,317.0		1,120
49 In	24,209.7	24,002.0	27,275.9	3,286.9	3,279.3	3,487.2	3,713.8	2,904.4
51 Sb	26,359.1	26,110.8	29,725.6	3,604.72	3,595.3	3,843.57	4,100.78	3,188.6

Appendix C

Diffraction patterns

Different orientations of a crystal can give different diffration patterns [Edington (1976)]. Fig. C.1 shows three diffraction patterns that were seen with the sample B, GaAsSb.
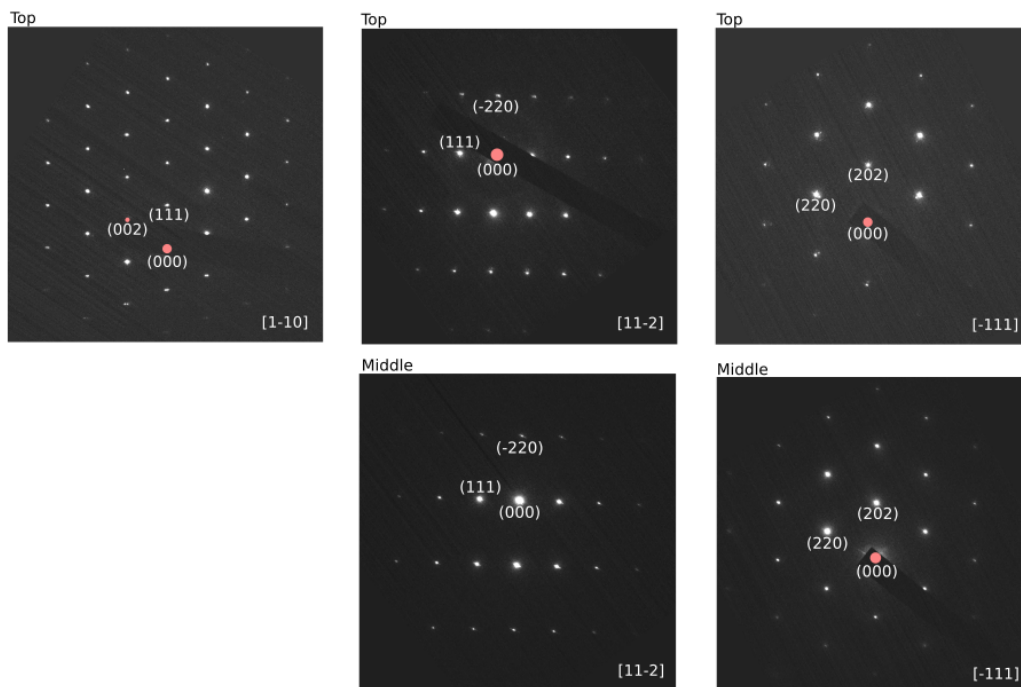
Figure C.1: Various DPs from the sample GaAsSb. Where the beam blocker covered some spots, they were drawn in with a red marker.

Appendix D

Hyperspy code

D.1 Conversion and scaling of raw EDS map data written by Adrian Lervik

```python
get_ipython().magic('matplotlib tk')
import hyperspy.api as hs
from pandas import read_csv
import re

# Load: .rpl, .msa and .txt
# .rpl = datafile from exported MAPDATA, .msa = energy
   calibration of single
# spectra and .txt = spatial calibration from an EDS-
   map metadata (details)
s = (hs.load('EDS_Data_10deg.rpl', signal_type="EDS_TEM
   ")).as_signal1D(0) spatial_calibration_rawdata =
   read_csv('text.txt', sep='\t', header=None)
single_spectra = hs.load('Map_Sum_Spectrum.msa',
   signal_type="EDS_TEM")

# Energy calibration
s.get_calibration_from(single_spectra)
s.axes_manager[2].name='Energy'
```

```python
# Scale should now be different from "1.0" [unitless],
    as it was initially.
# Should be "somevalue" [keV]
s.axes_manager[2].scale
# Spatial resolution calibration
column = ['2','3','4','5']
spatial_calibration = []
for i in column:
    a = [int(s) for s in re.findall(r'\d+', string=(
    spatial_calibration_rawdata.get_value(int(i),1,
        takeable=False)))]
    spatial_calibration.append(a[0])

# Variable: 'spatial_calibration' now include:
# 0 = Resolution_width,
# 1 = Resolution_height,
# 2 = Image_width,
# 3 = Image_height

names = ['x', 'y']
units = '$nm$'
scales = [spatial_calibration[2]/spatial_calibration
   [0], spatial_calibration[3]/spatial_calibration[1]]

for i in range(2):
    ax = s.axes_manager[i]
    ax.name = names[i]
    ax.units = units
    ax.scale = scales[i]

s.plot()

s.data.sum()

# Remember to save it!
s.save('edsmap', extension='hdf5')
```

D.2 Functions written by A. Garmannslund

```python
def determine_zeta_factor(s, intensities, composition,
    thickness, density):
    """
    Determine the zeta-factors from a sample with known
        mass-thickness and composition.
    Parameters
    ----------
    s: signal
        Temporary, replace later by self when moved to
            eds_tem.py
    intensities: list of signal
        The intensity for each X-ray line
    composition: list of float
        Composition of the elements in the same order
            as intensities.
    elements:
        Elements in same order as composition.
    mass_thickness: float or signal
        Mass-thickness for the sample. If signal, must
            be same shape as intensities.
    Returns
    -------
    A signal in the same shape as intensities, giving
        the zeta-factors for each X-ray line.
    """

    zfactors = utils.stack(intensities)
    zfactors.data = _determine_zeta_factor(zfactors.
        data, composition, s._get_dose("zeta"),
        thickness*1e-9*density)
    zfactors = zfactors.split()

    xray_lines = [xray.metadata.Sample.xray_lines[0]
        for xray in intensities]
```

```python
    for i, line in enumerate(xray_lines):
        zfactors[i].metadata.General.title = "Zeta-
            factor_for_" + line

    return zfactors

def _determine_zeta_factor(intensities, composition,
    dose, mass_thickness):
    """
    Determine zeta-factors
    Parameters
    ----------
    intensities: numpy.array
        The intensities for each X-ray line. The first
            axis should be the element axis.
    composition: list of float
        Composition of the elements given in weight-
            percent in the same order as intensities.
    dose: float
        Total electron dose given by i*t*N, where i is
            the beam_current, t is the acquisition time,
        and N the number of electrons per unit electric
            charge (1/e).
    Returns
    -------
    A numpy.array containing the zeta_factors with the
        same shape as intensities
    """

    zfactors = np.zeros_like(intensities, dtype=float)

    for i, (intensity, comp) in enumerate(zip(
        intensities, composition)):
        zfactors[i] = (dose * mass_thickness * comp) /
            intensity

    return zfactors
```

D.3   Zeta calibration

```
%matplotlib tk
import hyperspy.api as hs
import numpy as np
import scipy
import matplotlib.pyplot as plt
from pandas import read_csv
from hyperspy import utils


### Example GaAs ###

s_raw = hs.load('edsmap.hdf5') # Load the file.
s_raw.change_dtype('float')

s=s_raw.rebin(scale=[41,2,1]) # choose rebinning
rebin_var = 41*2 # change according to rebinning

lines = ["Ga_Ka","As_Ka"] # Add the x-ray lines to
    evaluate.
elements = ["Ga","Cu","As","C"] # Add all elements in
    the spectra. (To fit and deconvolute overlapp)
s.add_elements(['As', 'Ga', 'Cu', 'C' ]) # Cu and C are
     elements from the TEM grid
s.add_lines()
s.crop(axis=2, start=30) # crop zero peak

# Constants
probe_currents = 0.416 # Average (if measured before
    and after) in nA, depends on each measuring session
acquisition_time = 0.207*rebin_var # Dwell time in s
thickness = 88*np.cos(np.deg2rad(30))+0 # nm, change
    depending on tilt
density = 5317 # kg/m^3  GaAs
comp = hs.material.atomic_to_weight([0.5, 0.5], ("Ga",
    "As"))/100 # Mass fraction, order of elements the
    same as in 'lines'
```

```python
# Append it to the metadata
s.metadata.Acquisition_instrument.TEM.beam_current =
    probe_currents
s.metadata.Acquisition_instrument.TEM.Detector.EDS.
    real_time = acquisition_time

# This function does all the work. It creates a model
    including a background and all the elements in the
    sample
# fits the model and returns the intensities of the
    lines of interest. It returns the model and the
    zeta_factors
# for the desired line.
def run_analysis(s, acquisition_time, probe_current,
    thickness, density, lines, composition):
    s.add_lines(lines)
    s.add_elements(elements)
    m = s.create_model()
    m.fit_background()
    m.multifit()
    s_ints = m.get_lines_intensity(xray_lines=lines)
    zeta_factors = determine_zeta_factor(s, s_ints,
        composition, thickness, density)
    return m, zeta_factors

# Typicall usage
m, zeta_factors = run_analysis(s, acquisition_time,
    probe_currents, thickness, density, lines,
    composition=comp)

# Print the mean values
np.mean(zeta_factors[0].data.flatten())
for i in range(len(zeta_factors)):
    print ("Mean %s: %.2f" % (zeta_factors[i].metadata.
        General.title, np.mean(zeta_factors[i].data.
        flatten())))
```

D.4 Mapping with the CL- and ζ-method

```
### Example for GaAsSb ###

s_raw = hs.load('edsmap.hdf5') # Load the file.
s_raw.change_dtype('float')
s_raw.crop(axis=2, start=30) # crop zero peak

s_raw.decomposition(algorithm='nmf', output_dimension
    =4) # PCA with additional constraint of non-negative
     matrix factorisation
s=s_raw.get_decomposition_model()

lines = ["As_Ka","Ga_Ka","Sb_La"] # Add the x-ray lines
     to evaluate.
elements = ["As","Cu","Ga","C","Sb"] # Add all elements
     in the spectra. (To fit and devoncolute overlapp)


# Constants
probe_currents = 0.44 # changes at each measuring
    session
s.metadata.Acquisition_instrument.TEM.beam_current =
    probe_currents

# CL method
s.add_lines(lines)
s.add_elements(elements)
s.get_lines_intensity()

AsKa = s.get_lines_intensity()[0] # depending on
    elements, check the index
GaKa = s.get_lines_intensity()[1] # depending on
    elements, check the index
Sb_La = s.get_lines_intensity()[2] # depending on
```

```
    elements , check the index
intensities = [AsKa, GaKa, Sb_La]
intensities

kfactors = [1.636,1.444,1.935] # As_K,Ga_K,Sb_L # order
    alphabetically
# k=[3.475,1.045,1.444,1.693,1.636,1.674,1.876,1.935] #
    choose the k-factor given by AZtekEnergy: N_K,Al_K,
    Ga_K,Ga_L,As_K,As_L,In_L,Sb_L
compCL = s.quantification(intensities,'CL',kfactors,
    plot_result=True,composition_units='atomic')

# Zeta method
zetafactors = [1900,1800,5300] # As_K,Ga_K,Sb_L, choose
    for each sample
comp_s, pt_s = s.quantification(intensities,'zeta',
    zetafactors, plot_result=True,composition_units='
    atomic')

ts = get_thickness_map(comp_s, pt_s)
ts.plot() # plotting the thickness map
```